

Axonal Endoplasmic Reticulum Ca^{2+} Content Controls Release Probability in CNS Nerve Terminals

Highlights

- We report new highly sensitive genetically encoded ER-targeted Ca^{2+} sensors
- Neuronal activity drives net Ca^{2+} uptake into presynaptic ER
- ER Ca^{2+} handling integrity is critical for synaptic function
- $[\text{Ca}^{2+}]_{\text{ER}}$ drives a STIM1-based feedback loop to control Ca^{2+} influx and exocytosis

Authors

Jaime de Juan-Sanz, Graham T. Holt,
Eric R. Schreiter, Fernando de Juan,
Douglas S. Kim, Timothy A. Ryan

Correspondence

taryan@med.cornell.edu

In Brief

de Juan-Sanz et al. have developed novel, genetically encoded ER-targeted Ca^{2+} sensors to study ER Ca^{2+} fluxes in nerve terminals during electrical activity. Using these tools they demonstrate that ER Ca^{2+} content is critical for synaptic function and show that ER Ca^{2+} drives a STIM1-based feedback loop that controls Ca^{2+} influx and exocytosis.

Axonal Endoplasmic Reticulum Ca^{2+} Content Controls Release Probability in CNS Nerve Terminals

Jaime de Juan-Sanz,¹ Graham T. Holt,² Eric R. Schreiter,² Fernando de Juan,³ Douglas S. Kim,² and Timothy A. Ryan^{1,4,*}

¹Department of Biochemistry, Weill Cornell Medicine, New York, NY 10065, USA

²Janelia Research Campus, Howard Hughes Medical Institute, Ashburn, VA 20147, USA

³Department of Physics, University of Oxford, Oxford, OX1 3NP, UK

⁴Lead Contact

*Correspondence: taryan@med.cornell.edu

<http://dx.doi.org/10.1016/j.neuron.2017.01.010>

SUMMARY

Although the endoplasmic reticulum (ER) extends throughout axons and axonal ER dysfunction is implicated in numerous neurological diseases, its role at nerve terminals is poorly understood. We developed novel genetically encoded ER-targeted low-affinity Ca^{2+} indicators optimized for examining axonal ER Ca^{2+} . Our experiments revealed that presynaptic function is tightly controlled by ER Ca^{2+} content. We found that neuronal activity drives net Ca^{2+} uptake into presynaptic ER although this activity does not contribute significantly to shaping cytosolic Ca^{2+} except during prolonged repetitive firing. In contrast, we found that axonal ER acts as an actuator of plasma membrane (PM) function: $[\text{Ca}^{2+}]_{\text{ER}}$ controls STIM1 activation in presynaptic terminals, which results in the local modulation of presynaptic function, impacting activity-driven Ca^{2+} entry and release probability. These experiments reveal a critical role of presynaptic ER in the control of neurotransmitter release and will help frame future investigations into the molecular basis of ER-driven neuronal disease states.

INTRODUCTION

Although the existence of axonal ER has been well documented (Henkart et al., 1978; Tsukita and Ishikawa, 1976), how presynaptic ER dysfunction impacts synaptic function is poorly understood, making it difficult to understand how genetic lesions in ER proteins contribute to neurological disease states. For example, several axonopathies arise from mutations in ER proteins: genetic lesions in reticulon-2, REEP1, and atlastin-1 lead to hereditary spastic paraparesis, while mutations in VAP-B are causative agents in amyotrophic lateral sclerosis (Blackstone et al., 2011; Montenegro et al., 2012; Noreau et al., 2014; Teuling et al., 2007). Additionally, alterations of ryanodine receptor 2 are linked to cognitive dysfunction (Liu et al., 2012) and studies of the genetic loss of the γ -secretase complex strongly imply that certain pene-

trant mutations in familial Alzheimer's disease alter ER Ca^{2+} handling at nerve terminals (Zhang et al., 2009). One well-known function of the smooth ER is its role as a Ca^{2+} handling organelle, but there is little understanding of how perturbations in this process impact synaptic function (Verkhratsky, 2005). In general, ER Ca^{2+} store function can be separated into two roles: first, it can influence biochemical events by acting as a local source or sink of Ca^{2+} . Second, the ER can act as an actuator of plasma membrane (PM) function at ER-PM contacts, a function controlled by the Ca^{2+} concentration within the ER lumen ($[\text{Ca}^{2+}]_{\text{ER}}$). The best-established example of this second role is the activation of Orai, a PM- Ca^{2+} channel, by stromal interaction molecule 1 (STIM1), an ER- Ca^{2+} sensor (Hogan and Rao, 2015; Liou et al., 2005; Zhang et al., 2005), although a number of other PM targets of STIM1 have been identified (Hooper et al., 2013). One challenge in determining which role is operational is the absence of sufficiently sensitive tools to directly monitor $[\text{Ca}^{2+}]_{\text{ER}}$ during genetic, physiological, or pharmacological ER manipulations. This is particularly challenging in small compartments like axons, where the ER occupies an even smaller volume. In general, previous approaches aimed at understanding the role of axonal Ca^{2+} stores monitored only cytosolic Ca^{2+} during ER manipulations, not $[\text{Ca}^{2+}]_{\text{ER}}$ itself. To circumvent this problem and gain insight into how ER Ca^{2+} contributes to synaptic transmission, we designed and optimized genetically encoded ER-targeted Ca^{2+} sensors based on GCaMP, selected such that the affinity was lowered to match resting axonal $[\text{Ca}^{2+}]_{\text{ER}}$ but maintaining high responsiveness upon binding to Ca^{2+} . These new tools (ER-GCaMP6-150, ER-GCaMP6-210) allowed robust measures of Ca^{2+} dynamics in axonal ER during electrical activity for the first time and provided a precise approach to determine the consequences of pharmacological and genetic manipulations of ER function. These experiments demonstrated that resting $[\text{Ca}^{2+}]_{\text{ER}}$ levels are on average $\sim 150 \mu\text{M}$ but vary from cell to cell. This variation is correlated with presynaptic function, but this correlation depends on STIM1. Furthermore, pharmacological perturbations that lower $[\text{Ca}^{2+}]_{\text{ER}}$ and inhibit presynaptic Ca^{2+} influx and exocytosis also depend on STIM1 and its ability to sense Ca^{2+} via its luminal EF hand domain. Thus, ER Ca^{2+} content is a critical control parameter for neurotransmitter release and maintenance of ER health is essential for proper control of synaptic function.

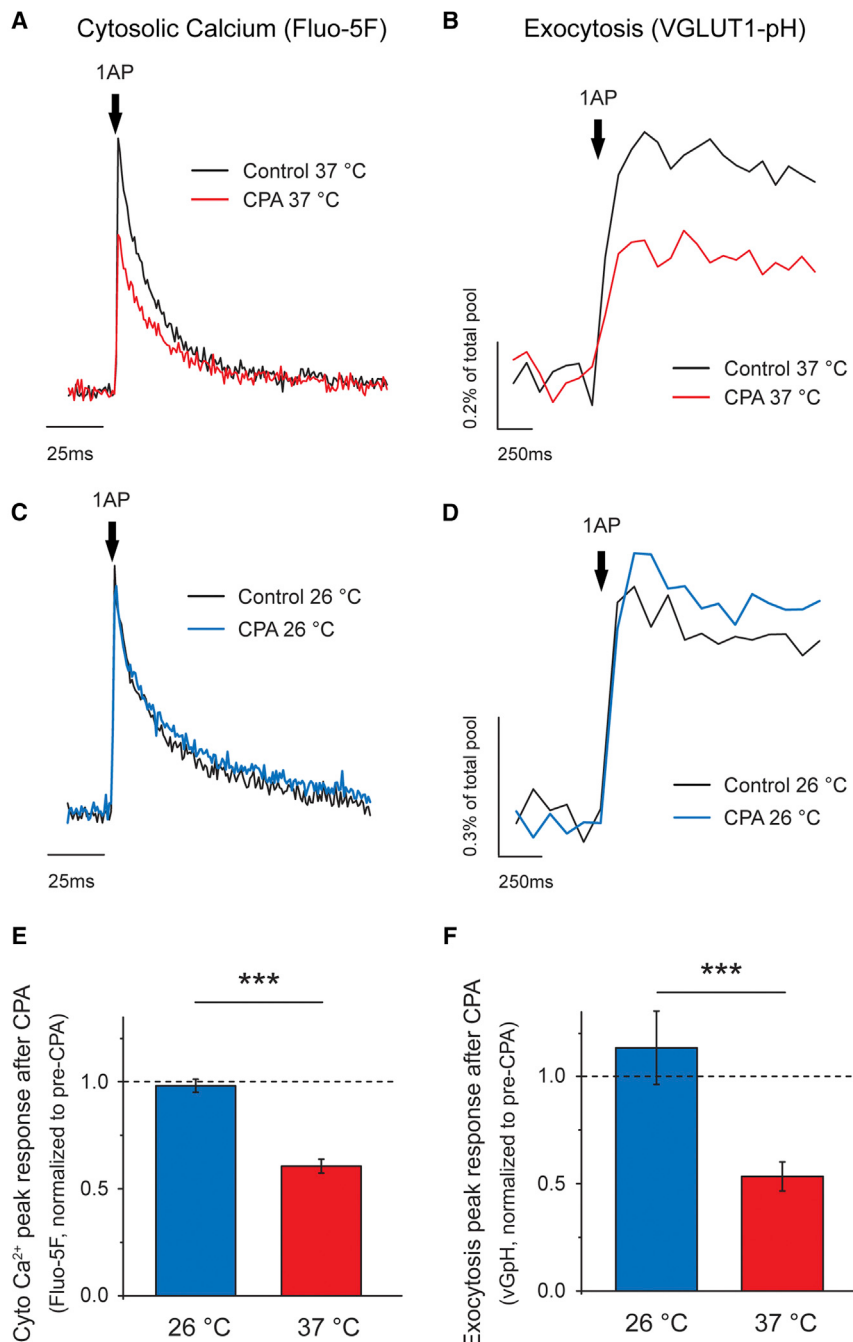


Figure 1. ER Ca²⁺ Handling Is Critical for Presynaptic Function at Physiological Temperature

(A–D) Representative traces of single AP presynaptic cytosolic Ca²⁺ responses measured using Fluo-5F AM (A and C) and vesicular exocytosis measured using vG-pH (B and D) before and after CPA treatment. Experiments were performed at 37 °C (A and B, shown in red) and 26 °C (C and D, shown in blue). Fluo-5F AM traces were normalized to the pre-CPA ΔF response (black trace). vG-pH responses are shown as percentage of their maximum fluorescence, obtained by brief perfusion of NH₄Cl buffered at pH 7.4.

(E and F) Differential effects observed are summarized by showing the remaining response after CPA treatment in each of the conditions (E and F): Fluo-5F AM, (26 °C) n = 10, (37 °C) n = 14; ***p = 1.44 · 10⁻⁷. vG-pH, (26 °C) n = 7, (37 °C) n = 10; ***p = 2.75 · 10⁻⁴. Error bars indicate ± SEM.

ATPases (SERCAs) impacts both presynaptic Ca²⁺ signals and exocytosis at nerve terminals in response to single action potential (AP) firing at 37 °C. Single AP-driven cytosolic Ca²⁺ signals arising from voltage-gated calcium channel (VGCC) opening at synaptic boutons were measured using Fluo-5F AM in regions identified with the presynaptic marker VAMP-mCherry (Calloway et al., 2015; Hoppa et al., 2012), whereas synaptic vesicle exocytosis was measured using the optical reporter VGLUT1-pHluorin (vG-pH) (Ariel et al., 2013; Armbruster and Ryan, 2011). We found that application of the potent SERCA inhibitor cyclopiazonic acid (CPA, 50 μM) led to a significant reduction in both single AP-driven Ca²⁺ signals (Figure 1A) and exocytosis (Figure 1B). Identical results were obtained using a genetically encoded Ca²⁺ indicator, GCaMP6f (Figure S1A), as well as with an alternative SERCA blocker, Thapsigargin (TG, 1 μM) (Figures S1B and S1C), making it unlikely that the reduction in Ca²⁺ signals is arising from an off-target effect. SERCA

blockade led to a small increase in baseline fluorescence in dendrites without a significant impact in axons (see STAR Methods and Figures S1D and S1E). Although such reduction in presynaptic Ca²⁺ signals during SERCA blockade has previously been reported in a number of synaptic preparations (Emptage et al., 2001; Liang et al., 2002), others concluded that similar manipulations of ER Ca²⁺ handling had little impact on presynaptic function (Carter et al., 2002). We noticed a striking correlation in the published literature regarding this issue: experiments performed at temperatures significantly colder (room temperature

RESULTS

Maintenance of Axonal ER Ca²⁺ Handling Is Critical for Presynaptic Function at Physiological Temperature

To examine ER's role in synaptic transmission and the behavior of ER Ca²⁺ during activity, we used primary dissociated hippocampal neurons as they allow using robust quantitative optical tools to dissect molecular function (Hoppa et al., 2012; Rangaraju et al., 2014). We examined how blocking the major ER Ca²⁺ influx pathway mediated by sarco/endoplasmic reticulum Ca²⁺-

22°C–26°C) than what would be physiological (37°C) for a rodent preparation observed that SERCA blockage had little impact on presynaptic function, whereas experiments performed at 30°C–32°C found a reduction in activity-driven Ca^{2+} signals. We repeated our measurements at a cooler temperature (26°C) and found that CPA had little impact on either AP-driven presynaptic Ca^{2+} entry (Figures 1C and 1E) or exocytosis (Figures 1D and 1F). Thus, the experimental temperature is critical for revealing the importance of ER Ca^{2+} handling in synaptic function and these experiments provide a plausible explanation for previous results that came to contradictory conclusions (Carter et al., 2002). The simplest interpretation of our results implies that the ER normally acts as a net source of Ca^{2+} during an AP, perhaps via calcium-induced Ca^{2+} release (CICR). However, the normally tight coupling of Ca^{2+} entry and exocytosis dictates that exocytosis is dominated by Ca^{2+} entry in the active zone restricted to domains near voltage-gated Ca^{2+} channels (Llinás et al., 1992; Stanley, 1997) and would unlikely be influenced by more distant sources of Ca^{2+} such as those from internal stores. In order to understand how ER Ca^{2+} handling could be impacting presynaptic function, we sought to directly examine ER Ca^{2+} dynamics.

A New Generation of Ultrasensitive ER Ca^{2+} Indicators

Understanding the biology of ER Ca^{2+} fluxes in axons and nerve terminals is currently constrained by the paucity of techniques suitable for detecting ER Ca^{2+} dynamics that arise in such small volumes. To solve this problem, we took advantage of a previous screening effort for generating novel genetically encoded calcium indicators (Chen et al., 2013) and focused on newly generated GCaMP variants that in vitro presented Ca^{2+} binding affinities reduced by a factor of ~500–1,000 but maintained high responsiveness upon binding to Ca^{2+} (i.e., high dynamic range). We selected four variants with different affinities to study further, which were divided in two classes depending on their responsiveness: GCaMP3 (dynamic range: 13–14) and GCaMP6 (dynamic range: 45–48). Each variant's name ends with a number that indicates its K_d for Ca^{2+} in μM . The variants used in this study are: GCaMP3-44, GCaMP6-150, GCaMP6-210, and GCaMP3-373 (Figure 2A; STAR Methods). Note that GCaMP3-373 is a variant previously published as GCaMPPer-10.19 (Henderson et al., 2015) but renamed here to maintain a comprehensive nomenclature. These variants were expressed in excitatory primary neurons under the CaMKII promoter and were specifically targeted to the ER using a well-established approach that is based on adding the N-terminal signal peptide of calreticulin and the C-terminal KDEL retention motif (Kendall et al., 1994; Kiyonaka et al., 2013; Miyawaki et al., 1997; Munro and Pelham, 1987) (see STAR Methods). High-resolution confocal imaging in cell somas expressing ER-targeted GCaMP6-150 (ER-GCaMP6-150) showed a detailed reticular network in the cell soma (Figure 2B) that extended throughout dendrites and the entire length of the axon including presynaptic boutons (Figure 2C).

Estimates of the Resting Ca^{2+} Concentration in Neuronal ER

In order to estimate $[\text{Ca}^{2+}]_{\text{ER}}$ in hippocampal excitatory neurons, we developed a protocol that relies on measuring the change in

fluorescence during indicator saturation by application of the Ca^{2+} ionophore ionomycin (see STAR Methods), which rapidly saturates ER-GCaMPs signals after 1–2 min of treatment (Figure 2D). To obtain a robust estimate of $[\text{Ca}^{2+}]_{\text{ER}}$, we applied this protocol to neurons separately expressing each of our four selected ER-GCaMP variants and measured somatic fluorescence changes. We found higher saturation peak values for the indicators with lower affinities (Figure 2E). Combined with the measured in vitro properties of the different indicators (Table S1), the fluorescence increase during ionomycin application allowed us to estimate the pre-ionomycin $[\text{Ca}^{2+}]_{\text{ER}}$ value (see STAR Methods). All four ER-GCaMP variants tested led to very similar estimates of resting $[\text{Ca}^{2+}]_{\text{ER}}$, ranging from 135 to 165 μM (average of the four estimates $152 \pm 8 \mu\text{M}$) (Figure 2F). These estimates were additionally corrected for the small change in ER pH induced by ionomycin (Figure S2A; see STAR Methods) that affects the fluorescence of each indicator differently depending on their pKa in the Ca^{2+} bound state (Table S1).

Action Potential Firing Drives a Net Ca^{2+} Uptake into the ER

To compare the ability of each indicator to detect physiological ER Ca^{2+} dynamics during AP firing, we used ER-GCaMPs and the previously published ER Ca^{2+} indicator G-CEPIA1er (Suzuki et al., 2014) to measure somatic ER Ca^{2+} handling during a brief burst of activity (20 AP at 20 Hz). In general, the net behavior of ER Ca^{2+} during activity will depend on the relative abundance of Ca^{2+} uptake mechanisms, such as those mediated by SERCAs, and ER Ca^{2+} efflux pathways, for example, mediated by IP₃ receptors and ryanodine receptors (Foskett et al., 2007; Liu et al., 2012), and the extent to which each of these are activated during a given stimulus. For the stimulus used here, a 1 s 20 AP burst, all indicators reported an increase in fluorescence indicating a net active uptake of calcium into somatic ER (Figures 3A–3C). The largest signals were obtained using ER-GCaMP6-150 and ER-GCaMP6-210 sensors, likely due to the better dynamic range and proximity of the affinities to resting $[\text{Ca}^{2+}]_{\text{ER}}$ of these probes (Figure 2A; Table S1). We verified that this level of activity does not impact ER pH in somas using an ER-targeted pHluorin (data not shown). In addition, we failed to detect any signal from these low-affinity Ca^{2+} indicators when expressed in the cytosol (for which the ER-targeting sequences were removed) (see below), indicating that these ER Ca^{2+} signals were not contaminated by any possible miss-targeted ER-GCaMPs in the cytosol.

We next examined both resting ER Ca^{2+} and activity-driven dynamics in nerve terminals in response to AP firing. Using the same procedures above, we measured $[\text{Ca}^{2+}]_{\text{ER}}$ in axons using ER-GCaMP6-150, of which the affinity for Ca^{2+} is best matched to the likely resting value (Table S1). These experiments showed that somatic and axonal $[\text{Ca}^{2+}]_{\text{ER}}$ values are not significantly different, as expected from the continuity of the organelle through the neuron (somatic $[\text{Ca}^{2+}]_{\text{ER}} = 164 \pm 7 \mu\text{M}$, $n = 8$; axonal $[\text{Ca}^{2+}]_{\text{ER}} = 156 \pm 15 \mu\text{M}$, $n = 15$, n.s. $p = 0.78$). Whether the ER at nerve terminals acts as a net source or sink for cytoplasmic Ca^{2+} during activity has been a subject of debate (Verkhratsky, 2005). We co-transfected hippocampal neurons with plasmids encoding each ER-GCaMP variant and VAMP-mCherry (Figures 2D

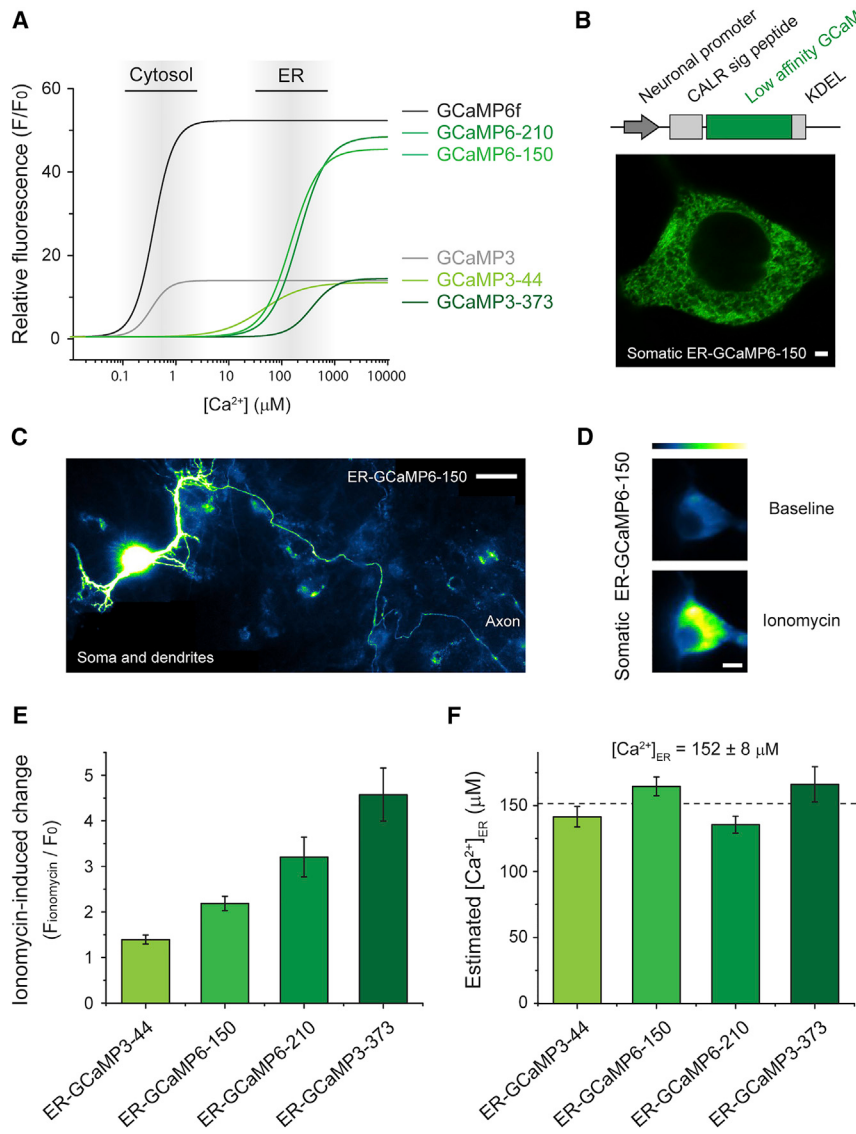


Figure 2. A New Generation of Ultrasensitive ER Ca^{2+} Indicators

(A) Predicted relative fluorescence versus Ca^{2+} curves based on binding parameters obtained in vitro (Table S1) of low-affinity calcium indicators GCaMP3-44, GCaMP6-150, GCaMP6-210, and GCaMP3-373 (light to dark green, high to low affinity) and high-affinity cytosolic indicators GCaMP3 (gray) and GCaMP6f (black). Approximate ranges of Ca^{2+} concentration in the cytosol and ER are indicated by gray gradient boxes. (B) Top: targeting scheme for expression in the neuronal ER by adding the N-terminal signal peptide of calreticulin (CALR sig peptide) and the C-terminal KDEL retention motif. Bottom: high-resolution image of somatic ER-GCaMP6-150 shows neuronal ER structure. Scale bar, 2 μm . (C) Montage of several fields from a neuron expressing ER-GCaMP6-150, which localizes in the ER network in the soma, dendrites and axons. Scale bar, 40 μm . (D–F) Neurons were treated with 500 μM ionomycin to induce indicator saturation for calibration. (D) Example pseudocolor images of somatic ER-GCaMP6-150 before and after ionomycin treatment. Pseudocolor scale shows low to high intensity. Scale bar, 8 μm . (E) Average peak fold-change in fluorescence ($F_{\text{ionomycin}}/F_0$) during ionomycin application for each ER-GCaMP. ER-GCaMP3-44, n = 14; ER-GCaMP6-150, n = 8; ER-GCaMP6-210, n = 9; ER-GCaMP3-373, n = 8; errors are $\pm\text{SEM}$. (F) pH-corrected estimate of resting ER calcium concentration based on each indicator saturation response. Dashed line indicates the average of the estimates from each of the indicators. Error bars indicate $\pm\text{SEM}$.

and 2E), which allows easy identification of nerve terminals. ER-GCaMP variants and G-CEPIA1er failed to reveal any signal during activity in nerve terminals (data not shown), whereas both ER-GCaMP6-150 and ER-GCaMP6-210 presented robust signals. Since resting $[\text{Ca}^{2+}]_{\text{ER}}$ is estimated to be $\sim 150 \mu\text{M}$, we carried out the majority of our subsequent experiments using ER-GCaMP6-150. These experiments showed that, similar to what was observed in somas, axonal ER acts a buffer for Ca^{2+} , rapidly taking up Ca^{2+} during AP firing (Figures 3D–3F; $\Delta F/F_0$ (20 AP) = 0.53 ± 0.04 , n = 64). Activity-driven increase in $[\text{Ca}^{2+}]_{\text{ER}}$ returned to baseline levels following a single exponential decay with an average decay constant of $\tau = 8.1 \pm 0.7 \text{ s}$. These experiments demonstrate that presynaptic ER acts as a net but transient sink during Ca^{2+} elevations driven by electrical activity. Single AP stimulation also resulted in net ER Ca^{2+} uptake (see below). These signals are ER specific since GCaMP6-150 expressed in the cytosol was not able to detect any response (cyto-GCaMP6-150, Figure 3F) and were not corrupted by po-

tential changes in ER pH as ER-pHluorin reported no pH changes in axonal ER during such brief bursts of stimulation (Figure S2B). Using our ionomycin-based estimate of the average resting $[\text{Ca}^{2+}]_{\text{ER}}$, the measured change in ER-GCaMP6-150 fluorescence ($\Delta F/F_0$) in response to 20 AP stimuli corresponds to an average transient increase in axonal $[\text{Ca}^{2+}]_{\text{ER}}$ of $\Delta [\text{Ca}^{2+}]_{\text{ER}} = 122 \pm 11 \mu\text{M}$ SEM (n = 64).

It is also possible to derive estimates of both resting $[\text{Ca}^{2+}]_{\text{ER}}$ and the change in $[\text{Ca}^{2+}]_{\text{ER}}$ during activity in somas and axons by comparing pairwise the average magnitude of the activity-driven increases in fluorescence obtained from probes with different affinities for Ca^{2+} (see STAR Methods). This approach does not make any assumptions about the ability of ionomycin to saturate the probes in the ER and relies only on using the measured in vitro properties of the different indicators and how these indicators respond to a given stimulus. Data obtained using this additional approach are summarized in Figure S3 and in general reveal broad agreement for the ionomycin and activity-based estimates. Our data thus strongly support the idea that at nerve terminals during brief AP firing the ER acts as net local sink for Ca^{2+} , not as a net local source.

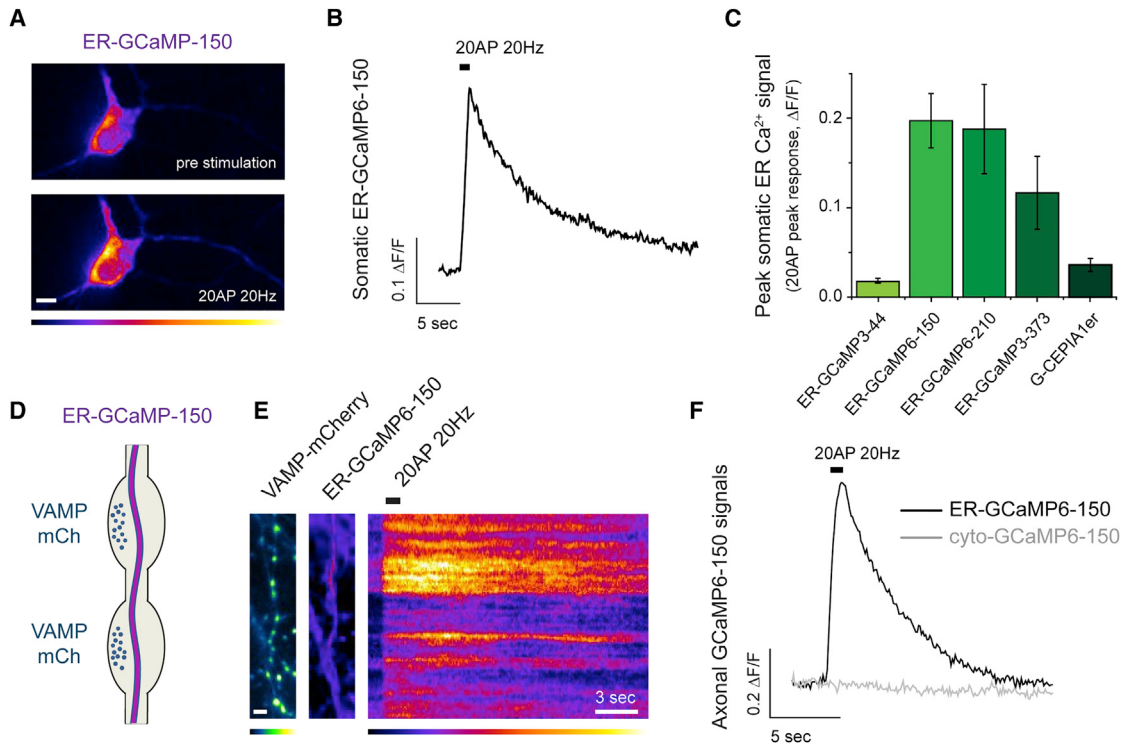


Figure 3. Neuronal Activity Drives ER Ca^{2+} Uptake

(A–C) Somatic ER Ca^{2+} responses to 20 AP (20 Hz) stimulation using different indicators. (A) Representative pseudocolor images of somatic ER-GCaMP6-150 before and after 20 AP (20 Hz) stimulation and (B) the corresponding fluorescence intensity over time (pseudocolor scale below showing low to high intensity). Scale bar, 8 μm . (C) Average of 20 AP peak somatic ER-GCaMP responses: G-CEPIA1er, $n = 5$; ER-GCaMP3-44, $n = 11$; ER-GCaMP6-150, $n = 12$; ER-GCaMP6-210, $n = 6$; ER-GCaMP3-373, $n = 11$; errors are $\pm \text{SEM}$.

(D) Diagram showing axonal ER crossing nerve terminals where ER Ca^{2+} responses were measured.

(E) ER-GCaMP-150 signals in presynaptic boutons identified by VAMP-mCherry expression (left, colored in green; scale bar, 4 μm) at rest (middle image) and during a 20 AP stimulus (displayed as a kymograph, right; pseudocolor scale shows low to high intensity). Scale bar, 3 s.

(F) Representative 20 AP presynaptic response measured with ER-GCaMP6-150 or cytosolic GCaMP6-150 (same variant without ER-targeting sequences).

Activity-Driven Ca^{2+} Uptake into Axonal ER Depends on SERCAs

In many cell types constitutive refilling of intracellular Ca^{2+} stores is pivotal for maintaining intracellular Ca^{2+} homeostasis and it is mediated by SERCAs. We verified that presynaptic ER Ca^{2+} uptake is mediated by SERCAs by examining the impact of pharmacological blockade of SERCAs on AP-driven ER Ca^{2+} signals. These experiments demonstrated that activity-driven transient increases in axonal $[\text{Ca}^{2+}]_{\text{ER}}$ driven by 20 AP (Figure 4A) or even one AP (Figure 4B) were eliminated by application of CPA. Single AP ER Ca^{2+} signals were measured using ER-GCaMP6-210, which provided a slightly better signal to noise ratio than ER-GCaMP6-150 in this regime. Furthermore, these data indicate that ER Ca^{2+} uptake appears to scale roughly linearly with stimulus number (single AP $\Delta[\text{Ca}^{2+}]_{\text{ER}} \sim 6 \mu\text{M}$, 20 AP $\Delta[\text{Ca}^{2+}]_{\text{ER}} \sim 120 \mu\text{M}$). Complete inhibition of ER Ca^{2+} uptake was also observed with the two other commonly used SERCA inhibitors, thapsigargin (TG, 1 μM) and 1,4-dihydroxy-2,5-di-tert-butylbenzene (BHQ, 50 μM) (Figure 4C). These results demonstrate that the transient uptake of Ca^{2+} into the ER during action potential firing requires SERCA function and suggest that the assumption that there is net release

of Ca^{2+} from the ER at nerve terminals during AP firing is incorrect.

Presynaptic Inhibition Is Slower than ER Ca^{2+} Depletion following SERCA Block

The fact that blocking ER Ca^{2+} handling inhibits cytosolic Ca^{2+} signals and exocytosis (Figure 1) even though the ER is not acting as a net source of Ca^{2+} in axons (Figure 4) implies that a more complex mechanism is linking presynaptic function at the plasma membrane to ER Ca^{2+} handling. To better understand the mechanism by which SERCA blockade modulates presynaptic plasma membrane function, we compared the time course of presynaptic $[\text{Ca}^{2+}]_{\text{ER}}$ and the time evolution of AP-triggered peak cytosolic Ca^{2+} during application of CPA. In neurons and other cell types, SERCA pump activity continuously counteracts Ca^{2+} leakage from the ER to the cytosol, resulting in balanced uptake/leak fluxes that maintain constant $[\text{Ca}^{2+}]_{\text{ER}}$ levels (Verkhatsky, 2005). Blocking ER Ca^{2+} uptake leads to $[\text{Ca}^{2+}]_{\text{ER}}$ depletion, a cellular dysregulation that is associated with many neurological disorders (Mekahli et al., 2011). We found that CPA application led to a depletion of axonal $[\text{Ca}^{2+}]_{\text{ER}}$ over a <1 min timescale both at 26°C ($\tau_{\text{ER depletion}} = 47.5 \pm 3.5$ s) and 37°C

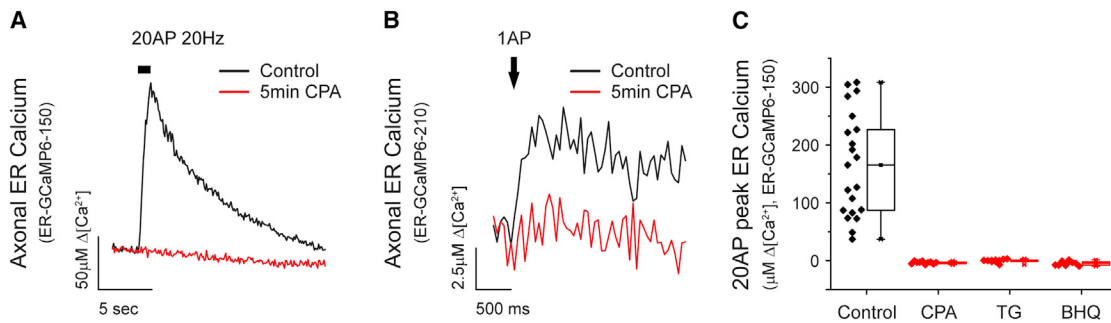


Figure 4. SERCA Function Is Necessary for Activity-Driven ER Ca^{2+} Uptake

(A and B) Representative presynaptic responses of (A) ER-GCaMP6-150 to 20 AP (20 Hz) or (B) ER-GCaMP6-210 to a single AP stimulus before and after 5 min of CPA (50 μM) application (black and red, respectively). Average of single AP $\Delta[\text{Ca}^{2+}]_{\text{ER}}$ responses before CPA was $5.9 \pm 1.3 \mu\text{M}$ ($n = 5$), which was reduced to $0.2 \pm 0.2 \mu\text{M}$ after CPA treatment ($n = 3$).

(C) Boxplots showing average and single-cell calibrated peak responses of neurons stimulated with 20 AP (20 Hz) before and after 5 min of treatment with CPA ($n = 10$), thapsigargin (TG, 1 μM , $n = 9$), or 1,4-dihydroxy-2,5-di-tert-butylbenzene (BHQ, 50 μM , $n = 9$).

($\tau_{\text{ER depletion}} = 26.0 \pm 0.9 \text{ s}$), with $[\text{Ca}^{2+}]_{\text{ER}}$ stabilizing to a new level of $\sim 100 \mu\text{M}$ in both cases ($\Delta[\text{Ca}^{2+}]_{\text{ER}}(26^\circ\text{C}) = -39 \pm 3 \mu\text{M}$, $\Delta[\text{Ca}^{2+}]_{\text{ER}}(37^\circ\text{C}) = -48 \pm 6 \mu\text{M}$), at which point any further activity-driven ER Ca^{2+} signals were eliminated (Figures 5A and 5B). The block of ER Ca^{2+} uptake had little impact on presynaptic single AP-driven Ca^{2+} signals at 26°C (Figures 5D and 5G) while at 37°C the reduction of cytosolic Ca^{2+} signals occurred at a 5- to 6-fold slower rate than the corresponding $[\text{Ca}^{2+}]_{\text{ER}}$ depletion (Figures 5E and 5H; $\tau_{\text{cyto Ca}^{2+}} = 148 \pm 18 \text{ s}$). The fact that modulation of presynaptic function is much slower than $[\text{Ca}^{2+}]_{\text{ER}}$ depletion implies that inhibition in exocytosis and AP-evoked Ca^{2+} signals are not simply due to loss of either an ER Ca^{2+} uptake or efflux pathway. Instead, it suggests that changing ER Ca^{2+} drives a slower control mechanism that is manifest at the plasma membrane. The absence of any impact on single AP-driven changes in Ca^{2+} after SERCA inhibition at 26°C (Figures 1C and 5D) also implies that the absolute ER Ca^{2+} fluxes at nerve terminals are likely small compared to single AP-triggered VGCC-mediated cytosolic Ca^{2+} entry and extrusion. In fact, block of ER Ca^{2+} uptake at 26°C only impacted Ca^{2+} accumulation during prolonged stimulus trains, leading to a modest increase in cytosolic Ca^{2+} discernible after 60 AP or more ($n = 8$, * $p < 0.05$; Figure S4A) and an increase in exocytosis observable only after 100 AP stimuli ($n = 7$, * $p = 0.03$; data not shown). Together, these data all provide strong evidence that although presynaptic ER can rapidly sequester cytosolic Ca^{2+} during activity, the direct impact on shaping cytosolic Ca^{2+} dynamics is relatively minor. Instead, our data reveal an unexpected feedback loop whereby the content of the ER drives a change in plasma membrane function (Figure 5) that is not apparent at a temperature only 11°C below the physiological temperature over a 10 min time period (Figure 5G).

Presynaptic Function Correlates with ER Ca^{2+} Content

The fact that reduced ER Ca^{2+} content results in the inhibition of Ca^{2+} influx and exocytosis at the plasma membrane (Figure 5) suggests that $[\text{Ca}^{2+}]_{\text{ER}}$ might be a key control parameter for presynaptic function. To test this idea, we measured axonal $[\text{Ca}^{2+}]_{\text{ER}}$ in individual neurons at 37°C and measured the corresponding

presynaptic single AP-evoked Ca^{2+} cytosolic signals in the same axons using the red Ca^{2+} indicator jRCaMP1b, which required increasing external Ca^{2+} up to 4 mM to improve signal to noise (Dana et al., 2016). Single AP stimulation resulted in an average $\Delta F/F$ change of 0.09 ± 0.01 , similar to previously reported (Dana et al., 2016), and its expression did not affect ER Ca^{2+} content (axonal $[\text{Ca}^{2+}]_{\text{ER}}$ when expressing jRCaMP1b = $169 \pm 8 \mu\text{M}$, n.s. $p = 0.43$ compared to control). Remarkably, these experiments revealed a significant correlation between ER Ca^{2+} content and presynaptic Ca^{2+} entry on a cell-by-cell basis (Spearman's correlation coefficient $\rho = 0.6$; * $p = 0.02$) (Figure S6A; see STAR Methods). To reduce observational noise found in the raw data (presented in Figure S6A), we binned these data, which allows obtaining a better estimate of the parameters in the fitting (Figure 6A; see STAR Methods). The correlation observed shows a saturable relationship and appears reasonably well described by a generalized Hill equation (see STAR Methods), with a Hill coefficient $n = 5.4$ and an apparent half maximal activation constant of $K_{1/2} \sim 105 \mu\text{M}$. The average drop in $[\text{Ca}^{2+}]_{\text{ER}}$ resulting from SERCA block ($\sim 50 \mu\text{M}$) also predicts a concurrent drop in Ca^{2+} influx of $\sim 45\%$, similar to what we observe experimentally ($\sim 35\%$; Figure 5F). These data support the idea that the natural variation in ER Ca^{2+} content across cells is a potential driver of synapse function via a feedback loop connecting ER Ca^{2+} and plasma membrane function. To test the veracity of this idea, we sought to determine (1) the key molecular driver of the feedback loop and (2) to examine both the correlation between ER Ca^{2+} and plasma membrane function and the impact of ER Ca^{2+} depletion when the feedback loop is disabled.

Loss of STIM1 Disables the Feedback Loop Linking ER Ca^{2+} Content to Presynaptic Ca^{2+} Influx and Exocytosis

In many cell types, ER Ca^{2+} is sensed by ER resident proteins belonging to the STIM family, which monitor Ca^{2+} store content via an ER-luminal low-affinity EF-hand domain. When ER Ca^{2+} is significantly lower than the Ca^{2+} affinity of STIM's Ca^{2+} binding domain, the unoccupied EF hand of STIM drives a conformational change that induces STIM clustering and activation (Liou et al., 2005; Zhang et al., 2005). This process is also strongly favored

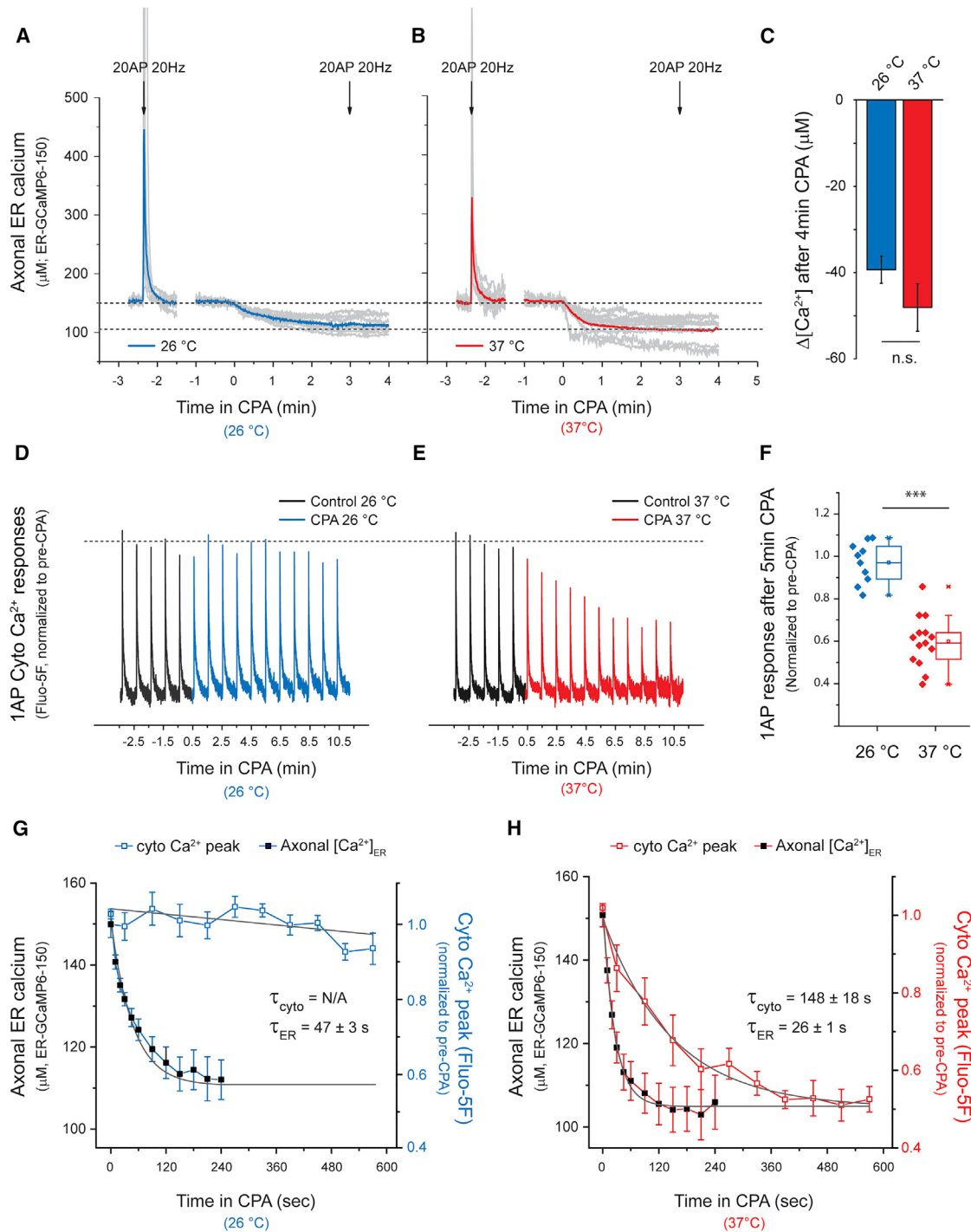


Figure 5. Presynaptic Inhibition Is Slower than ER Ca^{2+} Depletion following SERCA Block

(A–C) Average axonal ER Ca^{2+} dynamics were measured using ER-GCaMP6-150 at 26°C, (A, blue) or 37°C (B, red). Gray traces are individual experiments, although some individual responses overshot the scale used here and their peaks were not included in the graph. Neurons were stimulated with 20 AP (20 Hz) and then treated with CPA to induce ER Ca^{2+} depletion. After 3 min of CPA treatment, the responses to a second stimulus were abolished (indicated by second arrow, 20 AP 20 Hz). (C) Estimate of $\Delta[\text{Ca}^{2+}]_{\text{ER}}$ assuming an average resting $[\text{Ca}^{2+}]_{\text{ER}}$ based on ionomycin responses; $n(26^{\circ}\text{C}) = 8$, $n(37^{\circ}\text{C}) = 15$; n.s. $p = 0.36$. Error bars indicate $\pm \text{SEM}$. (D–H) Single-AP cytosolic Ca^{2+} responses (Fluo-5F AM, normalized to average pre-CPA ΔF response) every 60 s measured before (black traces) and after CPA treatment at 26°C (D and G, blue traces) or 37°C (E and H, red traces). (G and H) Comparison of the kinetics of presynaptic inhibition and axonal ER Ca^{2+} depletion. Curves were fit to single exponential decays where possible and time constants (τ) were obtained for comparison. $\tau_{\text{ER}}(26^{\circ}\text{C}) = 47.5 \pm 3.4 \text{ s}$, $n = 8$; $\tau_{\text{ER}}(37^{\circ}\text{C}) = 26 \pm 0.9 \text{ s}$, $n = 15$; $\tau_{\text{cyto } \text{Ca}^{2+}}(37^{\circ}\text{C}) = 148 \pm 18 \text{ s}$, $n = 7$. Error bars indicate $\pm \text{SEM}$.

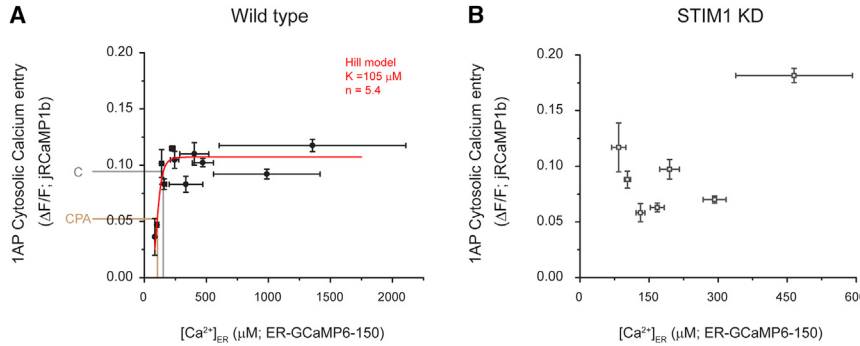


Figure 6. Presynaptic Ca^{2+} Influx Is Correlated with ER Ca^{2+} Content in Wild-Type but Not in STIM1 KD Neurons

(A and B) Neurons expressing ER-GCaMP6-150 and cytosolic jRCaMP1b were co-transfected with or without an shRNA targeting STIM1 and were used to examine single AP-driven Ca^{2+} influx (jRCaMP1b) and axonal $[\text{Ca}^{2+}]_{\text{ER}}$ (ER-GCaMP6-150) in the same cells. Recordings from wild-type ($n = 15$) and STIM1 KD ($n = 12$) neurons were grouped using a binning size of $[\text{Ca}^{2+}]_{\text{ER}} = 25 \mu\text{M}$ to better estimate fitting parameters (see STAR Methods; see Figure S6 for unbinned data). Errors of binned data points for $[\text{Ca}^{2+}]_{\text{ER}}$ and 1AP jRCaMP1b responses were calculated by

summing in quadrature the experimental estimates of SEM for each individual data point. These two variables are correlated only in wild-type cells (A) and are well described by a generalized Hill equation (red line) with a $K_{1/2}$ of $105 \mu\text{M} \pm 5 \mu\text{M}$ and a Hill coefficient of 5.4 ± 2.7 (Adjusted R-square = 0.87). Fitting in the case of STIM1 KD was not possible (B, see STAR Methods). Gray and brown lines show the predicted impact of CPA on Ca^{2+} influx when the average value of $[\text{Ca}^{2+}]_{\text{ER}}$ (152 μM) decreases by 48 μM , as measured during SERCA block.

at warmer versus colder temperatures (Xiao et al., 2011; Yarotsky and Dirksen, 2012) making it an attractive candidate for controlling the feedback between axonal ER Ca^{2+} and synaptic function. Although in immune cells activation of STIM1 leads to activation of plasma membrane Orai channels, activated STIM1 is thought to have alternate roles and different plasma membrane targets in neurons, including voltage-gated Ca^{2+} channels (Harraz and Altier, 2014; Park et al., 2010; Wang et al., 2010). Therefore, we explored whether STIM1 might be the molecular link underpinning the ER Ca^{2+} -presynaptic Ca^{2+} influx correlation (Figure 6A). We tested this idea in two ways. First, we examined whether ER Ca^{2+} content remains correlated with AP-driven Ca^{2+} influx in cells in which STIM1 expression was ablated. We co-expressed ER-GCaMP6-150 and jRCaMP1b with an shRNA targeting STIM1 that depleted STIM1 by $\sim 80\%$ (see STAR Methods; Figures S5A and S5B) and measured axonal $[\text{Ca}^{2+}]_{\text{ER}}$ and cytosolic 1AP-evoked Ca^{2+} signals. Remarkably, loss of STIM1 eliminated the correlation between ER Ca^{2+} content and AP-driven Ca^{2+} influx (Figure S6B; Spearman's correlation coefficient $p = -0.1$; n.s. $p = 0.97$) and no longer resembled a simple saturable relationship, even when the data are binned (Figure 6B), establishing that STIM1 plays a key role in the proposed feedback loop. Second, we examined how both AP-driven Ca^{2+} influx and exocytosis are impacted by ER Ca^{2+} depletion in neurons that lack STIM1. We co-expressed GCaMP6f (Figure 7A) or vG-pH (Figure 7B) with or without the shRNA targeting STIM1 and measured single AP-driven Ca^{2+} influx before and after CPA. We found that STIM1-KD neurons were almost completely resistant to CPA-induced changes in presynaptic function, whether analyzed as fractional or absolute changes induced by CPA (Figure 7A, Control $n = 16$, CPA effect = -0.34 ± 0.07 , *** $p = 0.0016$; STIM1-KD $n = 14$, CPA effect = -0.09 ± 0.05 , n.s. $p = 0.60$; see also Table S2). Loss of STIM1 did not impact resting cytosolic $[\text{Ca}^{2+}]_c$, axonal $[\text{Ca}^{2+}]_{\text{ER}}$ or its ability to be depleted during CPA treatment (Figures S5C–S5G). Furthermore, loss of CPA sensitivity was restored by re-expression of an shRNA-resistant variant of wild-type STIM1 (STIM1^{wt} $n = 10$, CPA effect = -0.31 ± 0.07 , * $p = 0.02$). Having established that STIM1 is an essential component to mediate ER Ca^{2+} content control of presynaptic function, we sought to determine whether it requires the

integrity of the Ca^{2+} -sensing EF hand of STIM1 that is in the ER lumen. In order to determine this, we attempted to rescue STIM1-KD neurons using a variant in which the critical Ca^{2+} coordinating residues of the EF hand were mutated (Liou et al., 2005; Zhang et al., 2005) (D76A and E87A, STIM1^{EF}) and examined the impact on CPA-mediated reduction of presynaptic Ca^{2+} influx. In contrast to the experiments performed with STIM1^{wt}, expressing STIM1^{EF} in STIM1-KD neurons (which correctly targets to axons, data not shown) did not restore CPA-mediated changes in presynaptic Ca^{2+} influx (STIM1^{EF} $n = 9$, CPA effect = 0.19 ± 0.10 , n.s. $p = 0.15$), indicating that STIM1's ability to sense ER Ca^{2+} concentration is essential for driving the feedback loop observed during ER Ca^{2+} depletion (Figures 7A and 7C). We also confirmed the role of STIM1 function in the reduction of activity-driven exocytosis during ER Ca^{2+} depletion by studying single AP responses of vG-pH under the same conditions (Figures 7B and 7D). As expected, whereas STIM1-KD neurons do not present CPA-induced modulation of vesicle fusion (STIM1-KD, $n = 8$, CPA effect = $+0.14 \pm 0.09$, n.s. $p = 0.23$), restored expression of STIM1^{wt} rescues the effect (STIM1^{wt} $n = 7$, CPA effect = -0.30 ± 0.04 , * $p = 0.031$) but only if STIM1 EF-hand Ca^{2+} binding sites are functional (STIM1^{EF} $n = 7$, CPA effect = $+0.11 \pm 0.11$, n.s. $p = 0.54$). Manipulations in STIM1 did not significantly impact basal release probability, although they did result in increased AP-evoked Ca^{2+} influx in the case of the STIM1-KD (Table S2). Although STIM1 has been shown to inhibit somatic L-type Ca^{2+} channels in neurons (Park et al., 2010; Wang et al., 2010), we find little evidence for their role in presynaptic Ca^{2+} influx as these signals are insensitive to the L-type calcium channel inhibitor isradipine ($n = 5$, effect = -0.07 ± 0.03 , n.s. $p = 0.80$) in agreement with previously published studies (Eggermann et al., 2011). Furthermore, the increase in presynaptic AP-evoked Ca^{2+} influx in STIM1-KD neurons was not due to a selective increase in the participation of a specific type of Cav2, as the relative sensitivity of these signals to both agatoxin or conotoxin (targeting Cav2.1 and Cav2.2, respectively) was similar to control neurons (WT, $n = 6$, agatoxin effect = -0.57 ± 0.04 , STIM1-KD, $n = 10$, agatoxin effect = -0.72 ± 0.04 , n.s. $p = 0.21$; WT, $n = 4$, conotoxin effect = -0.73 ± 0.05 , STIM1-KD, $n = 7$, conotoxin effect = -0.51 ± 0.06 , n.s. $p = 0.08$).

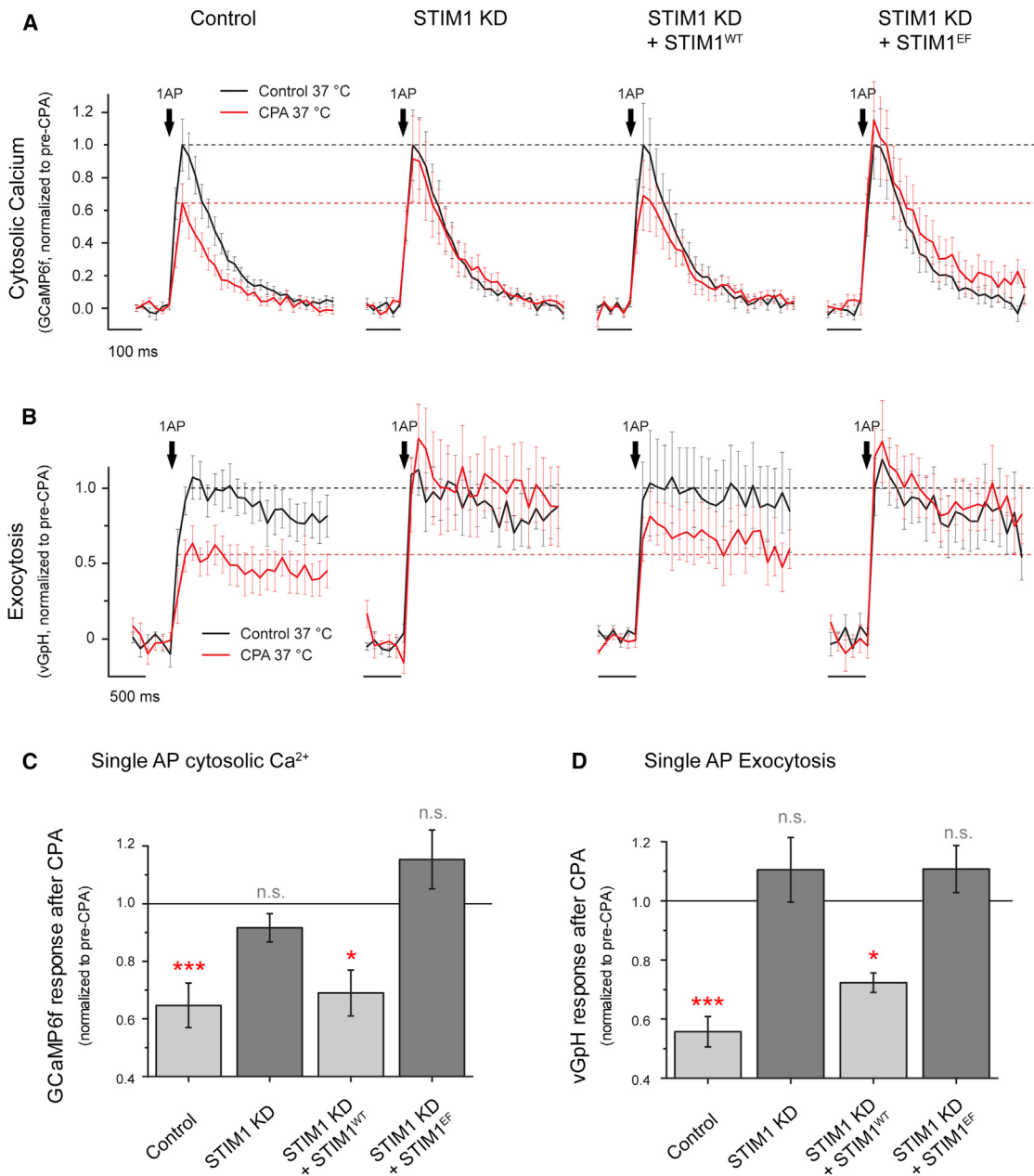
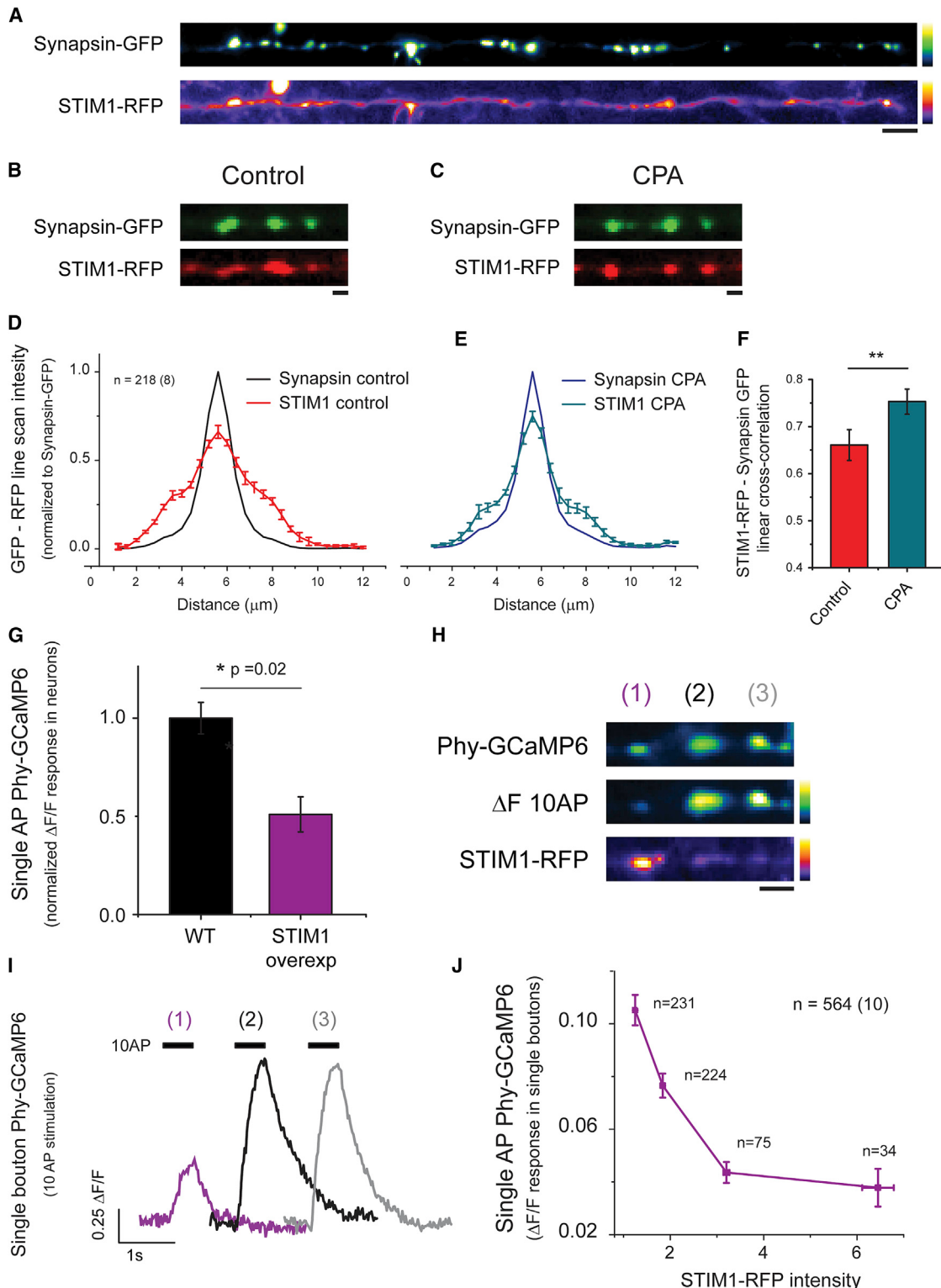


Figure 7. STIM1 Regulates Presynaptic Function Impairment Induced by ER Ca²⁺ Depletion

(A–D) Single AP-driven cytosolic Ca²⁺ signals and exocytosis were measured using GCaMP6f or vG-pH, respectively. Single AP-stimulated signals were quantified in wild-type neurons, STIM1 KD neurons, STIM1 KD neurons expressing an shRNA-resistant version of STIM1 (STIM1^{WT}), or STIM1 KD neurons expressing an shRNA-resistant version of STIM1 that is insensitive to ER Ca²⁺ content due to EF-hand mutations (STIM1^{EF}). Responses were quantified before (black) and after (red) CPA treatment. Black dashed lines represent average response before treatment, whereas red dashed lines represent the effect quantified in wild-type neurons for ease of comparison in the different conditions. (C and D) Differential effects of CPA are summarized by showing the remaining response after CPA treatment in each of the conditions. Solid black line indicates response before CPA treatment, normalized to 1 in each case. (C) Effects of CPA in single-AP-driven presynaptic Ca²⁺ signals, Control n = 16, ***p = 0.0016; STIM1 KD n = 14, n.s. p = 0.60; STIM1 KD + STIM1^{WT} n = 10, *p = 0.02; STIM1 KD + STIM1^{EF} n = 10, n.s. p = 0.14. (D) Effects of CPA in single AP vG-pH peak responses, Control n = 10, ***p = 6.68 · 10⁻⁵; STIM1 KD n = 7, n.s. p = 0.22; STIM1 KD + STIM1^{WT} n = 7, *p = 0.031; STIM1 KD + STIM1^{EF} n = 7, n.s. p = 0.55. Statistics were analyzed using paired sample Student's t test. Error bars indicate ± SEM.

**Figure 8. Local STIM1 Enrichment at Nerve Terminals Inhibits Ca^{2+} Influx**

(A) Representative image of an individual axon expressing STIM1-RFP and the presynaptic marker synapsin-GFP (straightened for ease of visualization). Vertical pseudocolor scales show low to high intensity. Black scale bar, 8 μm .

(B-E) Synapsin-GFP and STIM1-RFP were imaged before (B) and after CPA treatment (C). Scale bars, 2 μm .

(legend continued on next page)

Presynaptic STIM1 Is Enriched in Resting Nerve Terminals and Becomes Further Enriched during ER Ca²⁺ Depletion

Although our data indicate that STIM1 mediates a feedback loop linking ER Ca²⁺ and presynaptic function, our experiments did not explore whether this feedback is localized to nerve terminals. To examine this, we coexpressed STIM1-RFP and synapsin-GFP in individual neurons and examined their colocalization before and after ER Ca²⁺ depletion. Although STIM1-RFP is broadly distributed throughout axonal ER (Figure 8A), analysis of the local cross-correlation of STIM1-RFP with respect to synapsin-GFP fluorescence revealed that under resting conditions STIM1-RFP is enriched in nerve terminals (Figures 8B and 8D). This enrichment is consistent with the fact that the average value of [Ca²⁺]_{ER} (~150 μM) is reasonably close to the reported value of the affinity constant for Ca²⁺ binding to STIM1 (~180 μM) (Luik et al., 2008) and would predict that on average STIM1 would be in a partially activated state and thus recruited to interact with local plasma membrane binding partners. Furthermore, STIM1 presynaptic enrichment increased following ER Ca²⁺ depletion (Figures 8D–8F; Cross-correlation values; Control = 0.66 ± 0.03, CPA = 0.75 ± 0.02; **p = 0.0012) strengthening the idea that it provides a local feedback loop at the individual synapse level.

Local STIM1 Inhibits AP-Evoked Ca²⁺ Influx

Our analysis of presynaptic Ca²⁺ influx in STIM1 KD neurons suggests that even under resting conditions STIM1 is partially inhibiting presynaptic function. Furthermore, although we find that on average STIM1-RFP is enriched in resting nerve terminals, there is considerable variation in the relative abundance of STIM1-RFP across individual nerve terminals (Figure 8A). This variation suggests that nerve terminals might be in a differentially inhibited state even at rest. To test this hypothesis, we co-expressed STIM1-RFP and the genetically encoded, presynaptically targeted Ca²⁺ indicator synaptophysin-GCaMP6f (Phy-GCaMP6) and examined the correlation between the magnitude of AP-evoked Ca²⁺ influx and the local abundance of STIM1-RFP. On average, expression of STIM1-RFP lead to an ~50% inhibition of single AP-evoked Ca²⁺ influx compared to neurons transfected only with Phy-GCaMP6 (Figure 8G). These experiments also revealed a striking inverse correlation as illustrated by the example shown in Figures 8H and 8I of 3 en passant synapses along the same axon: higher abundance of STIM1-RFP was associated with synapses with a lower Ca²⁺ influx, while lower abundance of STIM1-RFP was associated with larger

presynaptic Ca²⁺ influx. This trend was borne out in a global analysis across a large population of boutons (564) across numerous neurons (10) and showed a strong inverse relationship between local STIM1-RFP abundance and AP-evoked Ca²⁺ influx (Figure 8J).

DISCUSSION

Modulation of nerve terminal Ca²⁺ influx is a potent lever for controlling neurotransmitter release as the coupling between these processes is non-linear (Schneggenburger and Neher, 2000). Our detailed measurements of [Ca²⁺]_{ER} dynamics uncovered a new control system that impacts presynaptic efficacy via a novel pathway whereby the status of [Ca²⁺]_{ER}, monitored by the ER Ca²⁺ sensing protein STIM1, controls AP-driven Ca²⁺ influx. The similarity of our observations with previous characterizations of presynaptic modulation after SERCA block in both acute (Liang et al., 2002) and organotypic neuronal slices (Emptage et al., 2001) at warm temperatures suggests that this ER Ca²⁺-based control of nerve terminal function is likely ubiquitous. Given that neuronal ER Ca²⁺ dyshomeostasis is proposed to be a pathological feature of many neurological disorders including Alzheimer's disease, amyotrophic lateral sclerosis (ALS), and Parkinson's disease (Bezprozvanny, 2009; Mekahli et al., 2011; Roussel et al., 2013; Stutzmann and Mattson, 2011), our data demonstrate a new link between ER dysfunction and synaptic dysfunction. It has long been speculated that ER Ca²⁺ handling is tightly associated with the control of mitochondrial ATP production (Csordás and Hajnóczky, 2009; Szabadkai and Duchen, 2008) and that the inability of mitochondria to produce ATP contributes significantly to the pathogenesis of many neurological disorders (Mattson et al., 2008). It is possible that the feedback loop we discovered here offers a protective mechanism that tamps presynaptic activity to reduce its corresponding energetic burden (Rangaraju et al., 2014) when ER function is compromised.

The protocols and measurement approaches described in this work should prove useful in examining the molecular basis of neuronal disease states associated with ER Ca²⁺ dyshomeostasis. Previous approaches for ER Ca²⁺ measurements (in cell somas) typically required manipulations that impact function (Alonso et al., 1998; Solovyova et al., 2002; Wu et al., 2013) or used genetically encoded Ca²⁺ indicators with insufficient sensitivity to detect axonal ER Ca²⁺ responses, including D1ER, LAR-GECO1, or G-CEPIA1er (Palmer et al., 2004; Suzuki et al., 2014; Wu et al., 2014). In contrast, ER-GCaMP6-150 and

(D–F) Intensity profiles of both proteins were analyzed in 218 individual boutons from 8 neurons and compared before and after 15 min of CPA treatment to obtain 1 dimensional intensity cross-correlation profiles, showing that the presynaptic enrichment of STIM1-RFP increases following CPA treatment (F; control = 0.66 ± 0.03, CPA = 0.75 ± 0.02; **p = 0.0012) with negligible impact on the distribution of synapsin-GFP (control, black profile in D; CPA, blue profile in E).

(G) Average decrease in single AP-Ca²⁺ influx following overexpression of STIM1-RFP.

(H) Representative image of a neuron co-transfected with Phy-GCaMP6 (top, left) and STIM1-RFP (bottom, left) showing the response to a 10 AP stimulus (middle, left). Note that nerve terminals with greater STIM1-RFP abundance (1) have lower Ca²⁺ influx than neighboring synapses (2, 3) with lower STIM1-RFP abundance (right). Vertical pseudocolor scales show low to high intensity. Black scale bar, 4 μm.

(I) Quantification of 10 AP-driven phy-GCaMP6 signals shown in (H).

(J) Quantification of single AP-driven phy-GCaMP6 signals and their corresponding STIM1-RFP intensities acquired from 564 individual boutons from 10 neurons co-transfected as in (H). STIM1-RFP intensities are shown as fluorescence normalized to the auto-fluorescence. Phy-GCaMP6 responses were binned into 4 different STIM1-RFP intensity groups (1–1.5, 1.5–2.5, 2.5–4.5, and >4.5) and reveal a strong inverse correlation between STIM1-RFP abundance and Ca²⁺ influx. Error bars indicate ± SEM.

ER-GCaMP6-210 appear optimal for ER Ca^{2+} measurements as their affinities are matched to resting $[\text{Ca}^{2+}]_{\text{ER}}$ and present remarkably high responsiveness. The unique properties of these probes allowed us to explore axonal ER Ca^{2+} handling's role and established several important aspects of axonal ER behavior: (1) neuronal activity drives net axonal ER Ca^{2+} uptake but not release, contrary to what has been hypothesized in previous work (Bouchard et al., 2003; Emptage et al., 2001; Liang et al., 2002; Nizami et al., 2010; Verkhratsky, 2005; Zhang et al., 2009), (2) axonal ER Ca^{2+} fluxes do not impact synaptic cytosolic Ca^{2+} levels except during prolonged activity, (3) decreases in axonal ER Ca^{2+} content trigger a temperature-dependent feedback loop that controls neurotransmitter release, and (4) this process is completely dependent on STIM1 and its ability to monitor neuronal ER Ca^{2+} content via its EF hands.

Several pieces of evidence support this novel role for STIM1. First, our estimates of resting $[\text{Ca}^{2+}]_{\text{ER}}$ suggest that changes in ER Ca^{2+} are poised to drive changes in STIM1 function since the estimates of EF hand affinity for Ca^{2+} binding in STIM1 ($\sim 180 \mu\text{M}$ [Luik et al., 2008]) are very similar to our estimates of neuronal $[\text{Ca}^{2+}]_{\text{ER}}$ ($\sim 150 \mu\text{M}$). Second, although in most cell types the apo-state of STIM1 drives an interaction that leads to the opening of plasma membrane Orai Ca^{2+} channels to replenish store Ca^{2+} content (Hogan and Rao, 2015), the role that such store-operated calcium entry (SOCE) plays in neurons is unclear since continuous activity-driven Ca^{2+} entry should provide sufficient cytosolic Ca^{2+} to replenish Ca^{2+} depleted stores (Moccia et al., 2015; Putney, 2003). Our work demonstrates net Ca^{2+} uptake into the ER during activity, consistent with this view. Furthermore, genetic deletion of STIM1 in neurons does not impair SOCE (Berna-Erro et al., 2009), even though neuronal ER Ca^{2+} depletion induces STIM1 clustering (Keil et al., 2010; Klejman et al., 2009; see also Figures 8B–8E). These results all support the notion that STIM1 activation in neurons has an alternate role when acting as an ER Ca^{2+} sensor (Harraz and Altier, 2014; Hooper et al., 2013; Majewski and Kuznicki, 2015; Moreno and Vaca, 2011). Third, STIM1 activation has been shown to be strongly favored at physiological versus colder temperatures (Xiao et al., 2011; Yarotskyy and Dirksen, 2012). Congruently, presynaptic function modulation during ER Ca^{2+} depletion is also highly temperature sensitive, while the ER Ca^{2+} depletion is not, suggesting that cold temperatures could affect the extent of STIM1 activation and impair its capacity to drive the feedback loop. Conditional and tissue specific genetic ablation of STIM1 in brain previously demonstrated that STIM1 is necessary for normal CNS function: forebrain STIM1 conditional knockout mice present significant learning defects (Garcia-Alvarez et al., 2015) and deletion of STIM1 in Purkinje neurons impairs cerebellar motor behavior (Hartmann et al., 2014). Given that STIM1 in neurons does not appear to be involved in SOCE (Berna-Erro et al., 2009), we speculate that the STIM1-mediated feedback onto the plasma membrane discovered here could be a regulatory process needed for normal neuronal and brain function.

It will be interesting in the future to elucidate mechanistic details of STIM1's control of Ca^{2+} influx and exocytosis and in particular to identify PM protein partners that allow STIM1 to control synaptic function during ER Ca^{2+} depletion, as several hypothetical PM targets are good candidates. STIM1 has been

shown to interact with the C terminus of Cav1 VGCC channels in neurons to suppress depolarization-induced channel opening during ER Ca^{2+} depletion (Park et al., 2010). Since it is unlikely that such putative interaction with Cav2 VGCCs would occur in the active zone, it would require Cav2 VGCCs to be sufficiently mobile to allow access to ER-PM junctions in order for STIM1 activation to drive Ca^{2+} influx inhibition via this mechanism. The latter possibility is supported by recent studies indicating that Cav2.1 and Cav2.2 are mobile and do not reside exclusively in the active zone (Heine et al., 2016; Schneider et al., 2015). Thus, activated STIM1 could potentially provide a trap that on average would increase the distance between vesicle release sensors and Ca^{2+} entry sites, in turn inhibiting neurotransmitter release. In this regard, it is interesting to note that the relationship in between changes in Ca^{2+} entry and exocytosis after CPA is not as steep as one would predict since the $\sim 35\%$ inhibition of AP-driven presynaptic Ca^{2+} entry after CPA application led to only an $\sim 45\%$ inhibition of exocytosis. Furthermore removal of STIM1 led to a significant increase in Ca^{2+} influx without a corresponding change in exocytosis. This suggests that following ER Ca^{2+} depletion the effective coupling of Cav2 channels to neurotransmitter release was altered and that STIM1 may play a role in controlling channels that are biased away from release sites. Alternatively, ER Ca^{2+} depletion could drive the interaction of STIM1 with other PM partners that alter phospho-inositol levels as has been suggested at certain ER-PM contacts (Saheki et al., 2016), which in turn could impact voltage-gated K^+ , Na^+ , or Ca^{2+} channel function. The fact that we see considerable heterogeneity in the local presynaptic abundance of STIM1-RFP suggests that additional local factors may in turn control the localization of STIM1 in presynaptic terminals.

Our results establish new principles of neuronal ER Ca^{2+} biology and synaptic function: presynaptic ER acts as a Ca^{2+} buffer during electrical activity but it also mediates a potent feedback loop acting on the plasma membrane that controls neurotransmitter release in a process mediated by the ER Ca^{2+} sensing protein STIM1. Additionally, the new generation of tools we introduce here should open new avenues for studying ER Ca^{2+} handling in numerous subcellular locales and tissues. This should be particularly useful to dissect the molecular basis for the control of ER Ca^{2+} and to identify the sources of variability in this parameter across different neurons, helping to understand the molecular basis of the many disease states associated with ER Ca^{2+} dyshomeostasis.

STAR★METHODS

Detailed methods are provided in the online version of this paper and include the following:

- KEY RESOURCES TABLE
- CONTACT FOR REAGENT AND RESOURCE SHARING
- EXPERIMENTAL MODEL AND SUBJECT DETAILS
 - Animals
 - Primary Neuronal Culture
- METHOD DETAILS
 - Inclusion and exclusion criteria of any data or subjects
 - Reagents

- Mutagenesis and selection of low affinity variants
 - Gene constructs
 - Live cell imaging
 - Image Analysis
 - ER calcium dynamics analysis and imaging
 - Immunocytochemistry
- QUANTIFICATION AND STATISTICAL ANALYSIS
- Baseline ER Calcium estimates
 - Cytosolic calcium analysis using GCaMP6f or jRCaMP1b
 - ER pH measurements
 - Analysis of correlation between $[Ca^{2+}]_{ER}$ and single AP Ca^{2+} entry
 - Estimates of contributions of ER efflux to resting cytosolic Ca^{2+}
 - Statistics
- DATA AND SOFTWARE AVAILABILITY

SUPPLEMENTAL INFORMATION

Supplemental Information includes six figures and two tables and can be found with this article online at <http://dx.doi.org/10.1016/j.neuron.2017.01.010>.

AUTHOR CONTRIBUTIONS

Experiments were designed by J.J.-S. and T.A.R. F.J. developed the quantitative procedures to estimate $[Ca^{2+}]_{ER}$. G.T.H. and E.R.S. characterized in vitro properties of purified low-affinity GCaMPs under the supervision of D.S.K. All other experiments were carried out by J.J.-S. The manuscript was written by J.J.-S. and T.A.R.

ACKNOWLEDGMENTS

This work was supported by a grant from the NIH (NS036942, MH0855783) to T.A.R. We thank Loren L. Looger and Jeremy Dittman for comments and Julia Marrs and Lucia A. Saidenberg for technical assistance. We thank the members of the Ryan lab for helpful discussion, especially Nimra Asi for her additional contribution to the statistical analysis and Geraldine Gouzer for generating the synaptophysin-GCaMP6f construct.

Received: June 3, 2016

Revised: November 23, 2016

Accepted: January 13, 2017

Published: February 2, 2017

REFERENCES

- Alonso, M.T., Barrero, M.J., Carnicero, E., Montero, M., Garcia-Sancho, J., and Alvarez, J. (1998). Functional measurements of $[Ca^{2+}]$ in the endoplasmic reticulum using a herpes virus to deliver targeted aequorin. *Cell Calcium* 24, 87–96.
- Ariel, P., Hoppa, M.B., and Ryan, T.A. (2013). Intrinsic variability in Pv, RRP size, $Ca(2+)$ channel repertoire, and presynaptic potentiation in individual synaptic boutons. *Front. Synaptic Neurosci.* 4, 9.
- Armbruster, M., and Ryan, T.A. (2011). Synaptic vesicle retrieval time is a cell-wide rather than individual-synapse property. *Nat. Neurosci.* 14, 824–826.
- Berna-Erro, A., Braun, A., Kraft, R., Kleinschmitz, C., Schuhmann, M.K., Stegner, D., Wultsch, T., Eilers, J., Meuth, S.G., Stoll, G., and Nieswandt, B. (2009). STIM2 regulates capacitive Ca^{2+} entry in neurons and plays a key role in hypoxic neuronal cell death. *Sci. Signal.* 2, ra67.
- Bezprozvanny, I. (2009). Calcium signaling and neurodegenerative diseases. *Trends Mol. Med.* 15, 89–100.
- Blackstone, C., O'Kane, C.J., and Reid, E. (2011). Hereditary spastic paraparesis: membrane traffic and the motor pathway. *Nat. Rev. Neurosci.* 12, 31–42.
- Bouchard, R., Patarini, R., and Geiger, J.D. (2003). Presence and functional significance of presynaptic ryanodine receptors. *Prog. Neurobiol.* 69, 391–418.
- Calloway, N., Vig, M., Kinet, J.P., Holowka, D., and Baird, B. (2009). Molecular clustering of STIM1 with Orai1/CRACM1 at the plasma membrane depends dynamically on depletion of Ca^{2+} stores and on electrostatic interactions. *Mol. Biol. Cell* 20, 389–399.
- Calloway, N., Gouzer, G., Xue, M., and Ryan, T.A. (2015). The active-zone protein Munc13 controls the use-dependence of presynaptic voltage-gated calcium channels. *eLife* 4, e07728.
- Carter, A.G., Vogt, K.E., Foster, K.A., and Regehr, W.G. (2002). Assessing the role of calcium-induced calcium release in short-term presynaptic plasticity at excitatory central synapses. *J. Neurosci.* 22, 21–28.
- Chen, T.W., Wardill, T.J., Sun, Y., Pulver, S.R., Renninger, S.L., Baohan, A., Schreiter, E.R., Kerr, R.A., Orger, M.B., Jayaraman, V., et al. (2013). Ultrasensitive fluorescent proteins for imaging neuronal activity. *Nature* 499, 295–300.
- Chi, P., Greengard, P., and Ryan, T.A. (2001). Synapsin dispersion and reclustering during synaptic activity. *Nat. Neurosci.* 4, 1187–1193.
- Csordás, G., and Hajnóczky, G. (2009). SR/ER-mitochondrial local communication: calcium and ROS. *Biochim. Biophys. Acta* 1787, 1352–1362.
- Dana, H., Mohar, B., Sun, Y., Narayan, S., Gordus, A., Hasseman, J.P., Tsegaye, G., Holt, G.T., Hu, A., Walpita, D., et al. (2016). Sensitive red protein calcium indicators for imaging neural activity. *eLife* 5, e12727.
- de Juan-Sanz, J., Núñez, E., López-Corcuera, B., and Aragón, C. (2013). Constitutive endocytosis and turnover of the neuronal glycine transporter GlyT2 is dependent on ubiquitination of a C-terminal lysine cluster. *PLoS ONE* 8, e58863.
- de Juan-Sanz, J., Núñez, E., Zafra, F., Berrocal, M., Corbacho, I., Ibáñez, I., Arribas-González, E., Marcos, D., López-Corcuera, B., Mata, A.M., and Aragón, C. (2014). Presynaptic control of glycine transporter 2 (GlyT2) by physical and functional association with plasma membrane Ca^{2+} -ATPase (PMCA) and Na^+ - Ca^{2+} exchanger (NCX). *J. Biol. Chem.* 289, 34308–34324.
- Eggermann, E., Bucurenciu, I., Goswami, S.P., and Jonas, P. (2011). Nanodomain coupling between Ca^{2+} channels and sensors of exocytosis at fast mammalian synapses. *Nat. Rev. Neurosci.* 13, 7–21.
- Emptage, N.J., Reid, C.A., and Fine, A. (2001). Calcium stores in hippocampal synaptic boutons mediate short-term plasticity, store-operated Ca^{2+} entry, and spontaneous transmitter release. *Neuron* 29, 197–208.
- Foskett, J.K., White, C., Cheung, K.H., and Mak, D.O. (2007). Inositol trisphosphate receptor Ca^{2+} release channels. *Physiol. Rev.* 87, 593–658.
- Garcia-Alvarez, G., Shetty, M.S., Lu, B., Yap, K.A., Oh-Hora, M., Sajikumar, S., Bichler, Z., and Fivaz, M. (2015). Impaired spatial memory and enhanced long-term potentiation in mice with forebrain-specific ablation of the Stim genes. *Front. Behav. Neurosci.* 9, 180.
- Harraz, O.F., and Altier, C. (2014). STIM1-mediated bidirectional regulation of $Ca(2+)$ entry through voltage-gated calcium channels (VGCC) and calcium-release activated channels (CRAC). *Front. Cell. Neurosci.* 8, 43.
- Hartmann, J., Karl, R.M., Alexander, R.P.D., Adelsberger, H., Brill, M.S., Rühlmann, C., Ansel, A., Sakimura, K., Baba, Y., Kuroski, T., et al. (2014). STIM1 controls neuronal Ca^{2+} signaling, mGluR1-dependent synaptic transmission, and cerebellar motor behavior. *Neuron* 82, 635–644.
- Heine, M., Ciuraszkiewicz, A., Voigt, A., Heck, J., and Bikbaev, A. (2016). Surface dynamics of voltage-gated ion channels. *Channels (Austin)* 10, 267–281.
- Henderson, M.J., Baldwin, H.A., Werley, C.A., Boccardo, S., Whitaker, L.R., Yan, X., Holt, G.T., Schreiter, E.R., Looger, L.L., Cohen, A.E., et al. (2015). A Low Affinity GCaMP3 Variant (GCAMPPer) for Imaging the Endoplasmic Reticulum Calcium Store. *PLoS ONE* 10, e0139273.
- Henkart, M.P., Reese, T.S., and Brinley, F.J., Jr. (1978). Endoplasmic reticulum sequesters calcium in the squid giant axon. *Science* 202, 1300–1303.

- Hogan, P.G., and Rao, A. (2015). Store-operated calcium entry: Mechanisms and modulation. *Biochem. Biophys. Res. Commun.* **460**, 40–49.
- Hooper, R., Samakai, E., Kedra, J., and Soboloff, J. (2013). Multifaceted roles of STIM proteins. *Pflugers Arch.* **465**, 1383–1396.
- Hoppa, M.B., Lana, B., Margas, W., Dolphin, A.C., and Ryan, T.A. (2012). $\alpha 2\delta$ expression sets presynaptic calcium channel abundance and release probability. *Nature* **486**, 122–125.
- Keil, J.M., Shen, Z., Briggs, S.P., and Patrick, G.N. (2010). Regulation of STIM1 and SOCE by the ubiquitin-proteasome system (UPS). *PLoS ONE* **5**, e13465.
- Kendall, J.M., Badminton, M.N., Dormer, R.L., and Campbell, A.K. (1994). Changes in free calcium in the endoplasmic reticulum of living cells detected using targeted aequorin. *Anal. Biochem.* **221**, 173–181.
- Kim, S.H., and Ryan, T.A. (2013). Balance of calcineurin A ζ and CDK5 activities sets release probability at nerve terminals. *J. Neurosci.* **33**, 8937–8950.
- Kim, J.H., Johannes, L., Goud, B., Antony, C., Lingwood, C.A., Daneman, R., and Grinstein, S. (1998). Noninvasive measurement of the pH of the endoplasmic reticulum at rest and during calcium release. *Proc. Natl. Acad. Sci. USA* **95**, 2997–3002.
- Kiyonaka, S., Kajimoto, T., Sakaguchi, R., Shimmi, D., Omatsu-Kanbe, M., Matsuura, H., Immamura, H., Yoshizaki, T., Hamachi, I., Morii, T., and Mori, Y. (2013). Genetically encoded fluorescent thermosensors visualize subcellular thermoregulation in living cells. *Nat. Methods* **10**, 1232–1238.
- Klejman, M.E., Gruszczynska-Biegala, J., Skibinska-Kijek, A., Wisniewska, M.B., Misztal, K., Blazejczyk, M., Bojarski, L., and Kuznicki, J. (2009). Expression of STIM1 in brain and puncta-like co-localization of STIM1 and ORAI1 upon depletion of Ca(2+) store in neurons. *Neurochem. Int.* **54**, 49–55.
- Liang, Y., Yuan, L.L., Johnston, D., and Gray, R. (2002). Calcium signaling at single mossy fiber presynaptic terminals in the rat hippocampus. *J. Neurophysiol.* **87**, 1132–1137.
- Liou, J., Kim, M.L., Heo, W.D., Jones, J.T., Myers, J.W., Ferrell, J.E., Jr., and Meyer, T. (2005). STIM is a Ca2+ sensor essential for Ca2+-store-depletion-triggered Ca2+ influx. *Curr. Biol.* **15**, 1235–1241.
- Liu, X., Betzenhauser, M.J., Reiken, S., Meli, A.C., Xie, W., Chen, B.X., Arancio, O., and Marks, A.R. (2012). Role of leaky neuronal ryanodine receptors in stress-induced cognitive dysfunction. *Cell* **150**, 1055–1067.
- Llinás, R., Sugimori, M., and Silver, R.B. (1992). Microdomains of high calcium concentration in a presynaptic terminal. *Science* **256**, 677–679.
- Luik, R.M., Wang, B., Prakriya, M., Wu, M.M., and Lewis, R.S. (2008). Oligomerization of STIM1 couples ER calcium depletion to CRAC channel activation. *Nature* **454**, 538–542.
- Majewski, L., and Kuznicki, J. (2015). SOCE in neurons: Signaling or just refilling? *Biochim. Biophys. Acta* **1853**, 1940–1952.
- Mattson, M.P., Gleichmann, M., and Cheng, A. (2008). Mitochondria in neuroplasticity and neurological disorders. *Neuron* **60**, 748–766.
- Mekahli, D., Bultynck, G., Parys, J.B., De Smedt, H., and Missiaen, L. (2011). Endoplasmic-reticulum calcium depletion and disease. *Cold Spring Harb. Perspect. Biol.* **3**, a004317.
- Miyawaki, A., Llopis, J., Heim, R., McCaffery, J.M., Adams, J.A., Ikura, M., and Tsien, R.Y. (1997). Fluorescent indicators for Ca2+ based on green fluorescent proteins and calmodulin. *Nature* **388**, 882–887.
- Moccia, F., Zuccolo, E., Soda, T., Tanzi, F., Guerra, G., Mapelli, L., Lodola, F., and D'Angelo, E. (2015). Stim and Orai proteins in neuronal Ca(2+) signaling and excitability. *Front. Cell. Neurosci.* **9**, 153.
- Montenegro, G., Rebelo, A.P., Connell, J., Allison, R., Babalini, C., D'Aloia, M., Montieri, P., Schüle, R., Ishiura, H., Price, J., et al. (2012). Mutations in the ER-shaping protein reticulon 2 cause the axon-degenerative disorder hereditary spastic paraparesis type 12. *J. Clin. Invest.* **122**, 538–544.
- Moreno, C., and Vaca, L. (2011). SOC and now also SIC: store-operated and store-inhibited channels. *IUBMB Life* **63**, 856–863.
- Munro, S., and Pelham, H.R. (1987). A C-terminal signal prevents secretion of luminal ER proteins. *Cell* **48**, 899–907.
- Nizami, S., Lee, V.W., Davies, J., Long, P., Jovanovic, J.N., and Sihra, T.S. (2010). Presynaptic roles of intracellular Ca(2+) stores in signalling and exocytosis. *Biochem. Soc. Trans.* **38**, 529–535.
- Noreau, A., Dion, P.A., and Rouleau, G.A. (2014). Molecular aspects of hereditary spastic paraparesia. *Exp. Cell Res.* **325**, 18–26.
- Oh-Hora, M., Yamashita, M., Hogan, P.G., Sharma, S., Lamperti, E., Chung, W., Prakriya, M., Feske, S., and Rao, A. (2008). Dual functions for the endoplasmic reticulum calcium sensors STIM1 and STIM2 in T cell activation and tolerance. *Nat. Immunol.* **9**, 432–443.
- Palmer, A.E., Jin, C., Reed, J.C., and Tsien, R.Y. (2004). Bcl-2-mediated alterations in endoplasmic reticulum Ca2+ analyzed with an improved genetically encoded fluorescent sensor. *Proc. Natl. Acad. Sci. USA* **101**, 17404–17409.
- Park, C.Y., Shcheglovitov, A., and Dolmetsch, R. (2010). The CRAC channel activator STIM1 binds and inhibits L-type voltage-gated calcium channels. *Science* **330**, 101–105.
- Putney, J.W., Jr. (2003). Capacitative calcium entry in the nervous system. *Cell Calcium* **34**, 339–344.
- Rangaraju, V., Calloway, N., and Ryan, T.A. (2014). Activity-driven local ATP synthesis is required for synaptic function. *Cell* **156**, 825–835.
- Roussel, B.D., Kruppa, A.J., Miranda, E., Crowther, D.C., Lomas, D.A., and Marciniak, S.J. (2013). Endoplasmic reticulum dysfunction in neurological disease. *Lancet Neurol.* **12**, 105–118.
- Saheki, Y., Bian, X., Schauder, C.M., Sawaki, Y., Surma, M.A., Klose, C., Pincet, F., Reinisch, K.M., and De Camilli, P. (2016). Control of plasma membrane lipid homeostasis by the extended synaptotagmins. *Nat. Cell Biol.* **18**, 504–515.
- Sankaranarayanan, S., De Angelis, D., Rothman, J.E., and Ryan, T.A. (2000). The use of pHluorins for optical measurements of presynaptic activity. *Biophys. J.* **79**, 2199–2208.
- Schneggenburger, R., and Neher, E. (2000). Intracellular calcium dependence of transmitter release rates at a fast central synapse. *Nature* **406**, 889–893.
- Schneider, R., Hosy, E., Kohl, J., Klueva, J., Choquet, D., Thomas, U., Voigt, A., and Heine, M. (2015). Mobility of calcium channels in the presynaptic membrane. *Neuron* **86**, 672–679.
- Solovyova, N., Veselovsky, N., Toescu, E.C., and Verkhratsky, A. (2002). Ca(2+) dynamics in the lumen of the endoplasmic reticulum in sensory neurons: direct visualization of Ca(2+)-induced Ca(2+) release triggered by physiological Ca(2+) entry. *EMBO J.* **21**, 622–630.
- Stanley, E.F. (1997). The calcium channel and the organization of the presynaptic transmitter release face. *Trends Neurosci.* **20**, 404–409.
- Stathopoulos, P.B., Zheng, L., Li, G.Y., Plevin, M.J., and Ikura, M. (2008). Structural and mechanistic insights into STIM1-mediated initiation of store-operated calcium entry. *Cell* **135**, 110–122.
- Stutzmann, G.E., and Mattson, M.P. (2011). Endoplasmic reticulum Ca(2+) handling in excitable cells in health and disease. *Pharmacol. Rev.* **63**, 700–727.
- Suzuki, J., Kanemaru, K., Ishii, K., Ohkura, M., Okubo, Y., and Iino, M. (2014). Imaging intraorganellar Ca2+ at subcellular resolution using CEPIA. *Nat. Commun.* **5**, 4153.
- Szabadkai, G., and Duchen, M.R. (2008). Mitochondria: the hub of cellular Ca2+ signaling. *Physiology (Bethesda)* **23**, 84–94.
- Teuling, E., Ahmed, S., Haasdijk, E., Demmers, J., Steinmetz, M.O., Akhmanova, A., Jaarsma, D., and Hoogenraad, C.C. (2007). Motor neuron disease-associated mutant vesicle-associated membrane protein-associated protein (VAP) B recruits wild-type VAPs into endoplasmic reticulum-derived tubular aggregates. *J. Neurosci.* **27**, 9801–9815.
- Tsukita, S., and Ishikawa, H. (1976). Three-dimensional distribution of smooth endoplasmic reticulum in myelinated axons. *J. Electron Microscop. (Tokyo)* **25**, 141–149.
- Verkhratsky, A. (2005). Physiology and pathophysiology of the calcium store in the endoplasmic reticulum of neurons. *Physiol. Rev.* **85**, 201–279.

- Voglmaier, S.M., Kam, K., Yang, H., Fortin, D.L., Hua, Z., Nicoll, R.A., and Edwards, R.H. (2006). Distinct endocytic pathways control the rate and extent of synaptic vesicle protein recycling. *Neuron* **51**, 71–84.
- Wang, Y., Deng, X., Mancarella, S., Hendron, E., Eguchi, S., Soboloff, J., Tang, X.D., and Gill, D.L. (2010). The calcium store sensor, STIM1, reciprocally controls Orai and CaV1.2 channels. *Science* **330**, 105–109.
- Wu, B., Yamaguchi, H., Lai, F.A., and Shen, J. (2013). Presenilins regulate calcium homeostasis and presynaptic function via ryanodine receptors in hippocampal neurons. *Proc. Natl. Acad. Sci. USA* **110**, 15091–15096.
- Wu, J., Prole, D.L., Shen, Y., Lin, Z., Gnanasekaran, A., Liu, Y., Chen, L., Zhou, H., Chen, S.R., Usachev, Y.M., et al. (2014). Red fluorescent genetically encoded Ca²⁺ indicators for use in mitochondria and endoplasmic reticulum. *Biochem. J.* **464**, 13–22.
- Xiao, B., Coste, B., Mathur, J., and Patapoutian, A. (2011). Temperature-dependent STIM1 activation induces Ca²⁺ influx and modulates gene expression. *Nat. Chem. Biol.* **7**, 351–358.
- Yarotskyy, V., and Dirksen, R.T. (2012). Temperature and RyR1 regulate the activation rate of store-operated Ca²⁺ entry current in myotubes. *Biophys. J.* **103**, 202–211.
- Zhang, S.L., Yu, Y., Roos, J., Kozak, J.A., Deerinck, T.J., Ellisman, M.H., Stauderman, K.A., and Cahalan, M.D. (2005). STIM1 is a Ca²⁺ sensor that activates CRAC channels and migrates from the Ca²⁺ store to the plasma membrane. *Nature* **437**, 902–905.
- Zhang, C., Wu, B., Beglopoulos, V., Wines-Samuelson, M., Zhang, D., Dragatsis, I., Südhof, T.C., and Shen, J. (2009). Presenilins are essential for regulating neurotransmitter release. *Nature* **460**, 632–636.
- Zheng, L., Stathopoulos, P.B., Schindl, R., Li, G.Y., Romanin, C., and Ikura, M. (2011). Auto-inhibitory role of the EF-SAM domain of STIM proteins in store-operated calcium entry. *Proc. Natl. Acad. Sci. USA* **108**, 1337–1342.

STAR★METHODS

KEY RESOURCES TABLE

REAGENT or RESOURCE	SOURCE	IDENTIFIER
Antibodies		
Rabbit anti-STIM1 antibody	Cell Signaling Technology	CAT#: 5668S, RRID: AB_10828699
Mouse Anti-MYC tag	Abcam	CAT#: ab18185, RRID: AB_444307
Chicken anti-GFP antibody	ThermoFisher Scientific	CAT#: A10263, RRID: AB_2534024
Chemicals, Peptides, and Recombinant Proteins		
Cyclopiazonic Acid	Alomone	CAT#: C-750
Fluo-5F, AM	ThermoFisher Scientific	CAT#: F14222
Ionomycin	Alomone	CAT#: I-700
Isradipine	Alomone	CAT#: I-100
ω-conotoxin-GVIA	Alomone	CAT#: C-300
ω-Agatoxin-IVA	Alomone	CAT#: STA-500
Thapsigargin	Tocris	CAT#: 1138
1,4-Dihydroxy-2,5-di-tert-butylbenzene (BHQ)	Tocris	CAT#: 1236
Critical Commercial Assays		
QuickChange site-directed mutagenesis kit	Agilent Technologies	CAT#: 210518
Experimental Models: Organisms/Strains		
Sprague-Dawley Rat	Charles River	Strain code: 400, RRID: RGD_734476
Recombinant DNA		
VGLUT-pHluorin	Voglmaier et al., 2006	N/A
STIM1-MYC	Oh-Hora et al., 2008	Addgene Plasmid #17732
STIM1-MYC (shRNA resistant)	This paper	N/A
D76A-E87A STIM1-MYC (shRNA resistant)	This paper	N/A
STIM1-RFP	Calloway et al., 2009	N/A
Synaptophysin-GCaMP6f	This paper	N/A
G-CEPIA1er	Suzuki et al., 2014	Addgene Plasmid #58215
ER-pHluorin	This paper	N/A
ER-GCaMP3-44	This paper	N/A
ER-GCaMP6-150	This paper	N/A
ER-GCaMP6-210	This paper	N/A
ER-GCaMP3-373	This paper	N/A
ER-GCaMP6-150 + STIM1 KD	This paper	N/A
jRCaMP1b	Dana et al., 2016	Addgene Plasmid #63136
GCaMP6f	Chen et al., 2013	Addgene Plasmid #40755
Synapsin-GFP	Chi et al., 2001	N/A
VAMP-mCherry	Hoppa et al., 2012	N/A
Sequence-Based Reagents		
STIM1 shRNA	Origene Technologies	CAT#: TR707032C
Software and Algorithms		
ImageJ	National Institute of Health	https://imagej.nih.gov/ij/
Mathematica 10	Wolfram	https://www.wolfram.com/mathematica/
OriginPro 8	OriginLab	http://www.originlab.com/
R	R Development Core Team	https://www.r-project.org/

(Continued on next page)

Continued

REAGENT or RESOURCE	SOURCE	IDENTIFIER
Other		
Custom program written for Mathematica (Wolfram) to easily propagate errors on ionomycin-based ER calcium estimates	This paper	https://github.com/jaimedejuan/Error-propagation-ER-Ca
Custom program written for Mathematica (Wolfram) to estimate baseline ER calcium comparing responses from 2 different indicators	This paper	https://github.com/jaimedejuan/pair-wise-indicator-calcium.git

CONTACT FOR REAGENT AND RESOURCE SHARING

Further information and requests for resources and reagents should be directed to and will be fulfilled by the Lead Contact Timothy A. Ryan at taryan@med.cornell.edu.

EXPERIMENTAL MODEL AND SUBJECT DETAILS**Animals**

All animal-related experiments were performed in accordance with protocols approved by the Weill Cornell Medicine IACUC. Wild-type rats were of the Sprague-Dawley strain (Charles River Strain code: 400, RRID: RGD_734476).

Primary Neuronal Culture

Hippocampal CA1-CA3 neurons were isolated from 1- to 3-day-old rats of mixed gender, plated on poly-ornithine-coated coverslips, transfected 7 days after plating, and imaged 14–21 days after plating as previously described. Neurons were maintained in culture media composed of MEM (Thermofisher Scientific S1200038), 0.6% glucose, 0.1 g/l bovine transferrin (Millipore 616420), 0.25 g/l insulin, 0.3 g/l glutamine, 5%–10% fetal bovine serum (Atlanta Biologicals S11510), 2% B-27 (Thermofisher Scientific 17504-044), and 4 µM cytosine β-d-arabinofuranoside. Cultures were incubated at 37°C in a 95% air/5% CO₂ humidified incubator for 14–21 days prior to use.

METHOD DETAILS**Inclusion and exclusion criteria of any data or subjects**

Fluorescence ER Ca²⁺ signals in response to electrical activity (ΔF) were normalized to the resting fluorescence (F_0). The F_0 value was additionally corrected for background autofluorescence measured in a nearby non-transfected region. To avoid overestimating $\Delta F/F_0$ which would arise in neurons with low F_0 values, we set an arbitrary threshold such that $F_0/\text{background} > 1.25$ to be included for further analysis. This threshold included 86.5% of all neurons tested in this study (64/74).

Reagents

All chemicals were obtained from Sigma except for cyclopiazonic acid (CPA (Alomone), thapsigargin and 1,4-dihydroxy-2,5-di-tert-butylbenzene (BHQ, Tocris), Fluo-5F, AM (Invitrogen), ionomycin (Alomone) and VGCC blockers isradipine, ω -conotoxin-GVIA and ω -Agatoxin IVA (Alomone).

Mutagenesis and selection of low affinity variants

Engineering of low affinity GCaMP variants presented in this study (STAR Methods) is part of the Genetically-Encoded Neuronal Indicator and Effector (GENIE) Project at Janelia Research Campus. Generation, selection and purification of low affinity GCaMPs was carried out as previously described (Chen et al., 2013) and the properties of the probes as a function of Ca²⁺ and pH were obtained as follows:

pH titrations

1.65 µl of purified protein in elution buffer (20 mM TRIS-HCl, pH 8.0, 100 mM NaCl, 100 mM imidazole) was added to 100 µl of pH titrated buffer (50 mM sodium citrate, 50 mM Tris, 50 mM glycine, 100 mM NaCl), containing either 5 mM EGTA or 50 mM CaCl₂, in duplicate. Fluorescence was measured in 96-well Greiner Bio-One transparent fluorescence plates in a Tecan Sapphire Spectrophotometer (Tecan), at 485 nm excitation and 510 nm emission, 5 nm slits, gain = 80 V.

Ca²⁺ titrations

Calcium affinity assays were performed by mixing different volumes of zero free calcium buffer (10 mM EGTA, 100 mM KCl, and 50 mM MOPS, pH 7.2) and 39 µM free calcium buffer (10 mM CaEGTA, 100 mM KCl, and 50 mM MOPS, pH 7.2). Extended calcium

range was performed by mixing different volumes of zero free calcium buffer (10mM NTA, 100mM KCl, and 50mM MOPS, pH 7.2) and 820 μ M free calcium buffer (10mM CaNTA, 100mM KCl, and 50mM MOPS, pH 7.2). Measurements were performed by adding 1.2 μ l of protein (~100 μ M) to 100 μ l of varying buffer ratios and measuring fluorescence in 96-well Greiner Bio-One transparent fluorescence plates in a Tecan Sapphire Spectrophotometer (Tecan), at 485 nm excitation and 510 nm emission, 5 nm slits, gain = 80 V.

Mutations in GCaMP3 to Generate Low-Affinity Ca^{2+} Indicators with High Sensitivity

Indicator	cpEGFP	Linker	Calmodulin										
GCaMP3-44	-	-	-	-	-	-	D362I	-	-	-			
GCaMP6-150	K78H	T302L	R303P	A317E	D324G	D360G	-	D380Y	T381R	S383T	R392G	-	-
GCaMP6-210	K78H	T302L	R303P	A317E	D324G	D360G	-	D380Y	T381R	S383T	R392G	D397G	-
GCaMP3-373	-	-	-	-	D324G	D360G	-	-	-	-	-	D397G	D435G

Mutations on GCaMP3 are performed in the circularly-permuted EGFP domain (cpEGFP), in the linker region, or in the calmodulin domain.

Gene constructs

To generate ER-GCaMPs and ER-pHluorin, selected low affinity GCaMP variants and pHluorin were targeted to the ER by adding a modified N terminus signal peptide from human calreticulin (MGLLSVPLLLGLLGLAVA-) followed by a short linker (TGGG) and a C terminus KDEL retention motif preceded by a short linker (GGSAGGG). All variants present a Kozak sequence (GCCGCCACC) before the initial ATG. Nucleotide sequences containing ER targeting and GCaMPs/pHluorin were optimized in silico for mouse protein expression, synthesized in vitro (Life Technologies) and cloned into the BamHI and EcoRI sites of the CaMKII promoter vector, which was a gift from Edward Boyden (Addgene plasmid #22217). G-CEPIA1er was a gift from Masamitsu Iino (Addgene plasmid # 58215). STIM1-shRNA vector was obtained from Origene (#TR707032C) and uses the RNAi-targeting sequence GGATAATGGCTCTATTGGTGAGGAGACAG. STIM1-MYC construct (Oh-Hora et al., 2008) was a gift from Anjana Rao (Addgene plasmid # 17732) and was used as a template for generating an shRNA-resistant version of STIM1 and the D76A-E87A EF mutant using site-directed mutagenesis (Agilent Technologies) as previously described (de Juan-Sanz et al., 2013). STIM1-RFP construct (Calloway et al., 2009) was a gift from Barbara A. Baird and David Holowka (Cornell University). Synaptophysin-GCaMP6f (phy-GCaMP6) was generated by adding GCaMP6f to the C terminus of the mouse sequence of synaptophysin as previously reported (Kim and Ryan, 2013). Synapsin-GFP and VAMP-mCherry were previously cloned in the laboratory (Chi et al., 2001; Hoppa et al., 2012). To facilitate co-expression of STIM1-KD shRNA and ER-GCaMP6-150 in experiments that required triple transfections, a U6 promoter and its following shRNA sequence targeting STIM1 were amplified by PCR and cloned into a single PciI site on the ER-GCaMP6-150 vector.

Live cell imaging

Calcium phosphate-mediated gene transfer was used to transfet 6–8-day-old cultures as described previously (Sankaranarayanan et al., 2000). Live-cell imaging was performed using a custom-built laser illuminated epifluorescence microscope with an Andor iXon+ (model #DU-897E-BV) back-illuminated electron-multiplying charge-coupled device camera. Experiments were performed at a clamped temperature of 37°C (or 26°C when noticed) using a custom-built objective heater under feedback control. Action potentials were evoked by passing 1-ms current pulses, yielding fields of approximately 10 V cm⁻¹ via platinum-iridium electrodes. Cells were continuously perfused at 0.1 ml min⁻¹ with a Tyrode's solution containing (in mM) 119 NaCl, 2.5 KCl, 1.2 CaCl₂, 2.8 MgCl₂, 30 glucose, 10 μ M 6-cyano-7-nitroquinoxaline-2,3-dione (CNQX) and 50 μ M D,L-2-amino-5-phosphonovaleric acid (AP5), buffered to pH 7.4 using 25 mM HEPES. In the case of single AP VGLUT1-pHluorin (vG-pH) experiments, CaCl₂ was increased to 2mM and MgCl₂ reduced to 2mM to facilitate exocytosis and improve signal-to-noise (Ariel et al., 2013; Voglmaier et al., 2006). vG-pH signals are reported as a percentage of the total vesicle pool, whose fluorescence is obtained by perfusion of a Tyrode's solution containing 50mM NH₄Cl buffered at pH 7.4 using 25mM HEPES (Sankaranarayanan et al., 2000). In the case of single AP jRCaMP1b experiments, CaCl₂ was increased to 4mM and MgCl₂ reduced to 0mM to improve signal-to-noise. During experiments cells were allowed to rest for ~60 s between single action potential trials and at least 5 min between 20–100 action potential bursts. In order to obtain robust estimates for vG-pH, GCaMP6f, Fluo-5F AM, jRCaMP1b and ER-GCaMP6-210 single AP signals, responses were averaged over several trials performed every 60 s (vG-pH, 12; GCaMP6f, 8–10; Fluo-5F AM, 1–3; jRCaMP1b, 10–12; ER-GCaMP6-210, 15). In the case of CPA or Thapsigargin treatments in neurons expressing GCaMP6f or vG-pH, cells were treated during 5min with a SERCA blocker and then assayed for single AP responses every 60 s during the next 10–12 min of treatment, showing the final effect as the average of those trials during treatment. Cytosolic calcium (both Fluo-5F AM and GCaMP6f) experiments were imaged at 50Hz whereas vG-pH experiments were imaged at 10Hz. Fluo-5F AM measurements were performed by loading cells with 1 μ g Fluo-5F AM at 37°C for 10 min followed by a 10 min wash and approximately 5 min equilibration at 37°C. In Fluo-5F AM experiments AP-driven Ca^{2+} entry signals and changes associated with CPA treatment are reported as ΔF signals since we observed a small increase in baseline fluorescence during

SERCA blockade that arose primarily from surrounding dendrites. Using GCaMP6f in individual neurons we confirmed that axonal baseline fluorescence is not impacted during SERCA blockade (Figure S1A, B) and confirmed the CPA effect on single-AP stimulated Ca^{2+} entry (Figure 1C). High resolution images of ER-targeted low-affinity GCaMP variants in live neurons were acquired using a Zeiss 63x (0.75NA) LD Plan-Neofluar objective in an inverted Zeiss LSM 880 laser scanning confocal microscope with AiryScan.

Image Analysis

Images were analyzed using the ImageJ plugin Time Series Analyzer V3 where typically 10-20 regions of interest (ROIs) corresponding to synaptic boutons, axonal regions or cell somas as appropriate were selected and the fluorescence was measured over time. All fitting was done with OriginPro v8. Statistical analysis was performed with OriginPro v8 or R.

ER calcium dynamics analysis and imaging

ER-targeted low affinity GCaMP variants were used to measure somatic and presynaptic bouton ER Ca^{2+} dynamics. ER-GCaMP peak fluorescence ($\Delta F/F_0$) for each stimulation was found by averaging the 3 highest points divided by the average pre-stimulus fluorescence time points. ER calcium was generally imaged at 10Hz except for single AP responses (20Hz) and SERCA-block-induced ER depletion experiments (2Hz). ER calcium decay after stimulation and ER calcium depletion follow a single exponential decay, which decay constants (τ) were calculated using Origin 8.0 (LabCorp). 20AP (20Hz) experiments included in the present dataset reached at least an R-squared value of 0.95 for exponential decay fitting and a signal to noise ratio of at least 10 for the peak response over the baseline fluctuation. In addition, to avoid overestimating $\Delta F/F_0$ signals in neurons presenting low F_0 values, we set an arbitrary threshold in which $F_0/\text{background} > 1.25$. This threshold includes 86.5% of all neurons tested in this study (64/74).

Immunocytochemistry

To quantify endogenous STIM1 expression and measure knockdown efficiency, primary neurons expressing cytosolic GFP alone or in combination with STIM1 shRNA vector were analyzed by immunocytochemistry: after 4% PFA fixation, neurons were blocked and permeabilized for 90 min at room temperature in 0.3% Triton X-100, 10% normal goat serum and 1% BSA, and stained with antibodies overnight at 4°C against STIM1 (rabbit, Cell Signaling, #5668; 1:800) and GFP (chicken, Life Technologies, #A10262, 1:1000). Samples were then incubated for 1 hr at RT with Alexa-546 anti-rabbit and Alexa 488 anti-chicken secondary antibodies (Life Technologies). STIM1 expression levels were determined by quantifying the Alexa-546 fluorescence in somas of transfected neurons identified by GFP labeling. These values were corrected against local background staining and compared to neighboring untransfected somas to correct for variations in global staining intensity. Immunocytochemistry to ensure expression of STIM1-MYC or D76A/E87A STIM1-MYC in STIM1-KD neurons using an antibody against the myc tag (mouse, Abcam, #ab18185; 1:500) was performed as described previously (de Juan-Sanz et al., 2014), visualized using an Alexa-546 anti-mouse secondary antibody (Life Technologies).

QUANTIFICATION AND STATISTICAL ANALYSIS

Baseline ER Calcium estimates

We have developed two different methods for estimating ER calcium concentrations in neurons using low affinity GCaMPs.

Method 1 – Pharmacological saturation

This method relies on the experimental measurement of ER-GCaMP fluorescence at saturating $[\text{Ca}^{2+}]_{\text{ER}}$ (F_{max}), which is obtained by applying Tyrode's solution containing ionomycin at pH 6.9 buffered with 25mM HEPES. Different ionomycin concentrations were used depending on the neuronal compartment: 500 μM (soma) or 50 μM (axon). Knowing the in vitro characteristics of the indicator used (Table S1), baseline $[\text{Ca}^{2+}]_{\text{ER}}$ (Ca_r) is calculated from F_{max} using the following equation:

$$[\text{Ca}]_r = K_d \left(\frac{F_r/F_{\text{max}} - 1/R_f}{1 - F_r/F_{\text{max}}} \right)^{1/n} \quad (\text{Eq. 1})$$

K_d is the affinity constant of the indicator, F_r is the measured fluorescence at rest, R_f is the dynamic range ($F_{\text{sat}}/F_{\text{apo}}$) and n is the Hill coefficient. Ionomycin application produces a change in ER pH (axons, 50 μM : 7.24 to 7.35; somas 500 μM : 7.24 to 7.68) that affects F_{max} depending on the pH responsiveness of the calcium-bound form of the indicator used (driven by its $pK_a(\text{sat})$ and the Hill coefficient factor of the pH dependence). Therefore, the final F_{max} value for each indicator is corrected for a different pH variation. We have estimated the percentage contribution of pH change to fluorescence change for each indicator during ionomycin treatments and subtracted those values from F_{max} in each case before estimating ER calcium concentration. The error in the determination of $[\text{Ca}^{2+}]_{\text{ER}}$ was assumed to arise from errors associated from the measurement of the relative fluorescence change obtained in the presence of ionomycin, $f = F_{\text{max}}/F_r$ as

$$\Delta[Ca]_r = \left| \frac{\partial[Ca]_r}{\partial f} \right| \Delta f \quad (\text{Eq. 2})$$

With

$$\frac{\partial[Ca]_r}{\partial f} = \frac{K_d(-1 + R_f) \left(\frac{f - R_f}{R_f - fR_f} \right)^{1/n}}{n(-1 + f)(f - R_f)} \quad (\text{Eq. 3})$$

We used a custom program written for Mathematica (Wolfram) to easily propagate these errors, which can be found at <https://github.com/jaimedejuan/Error-propagation-ER-Ca>.

Method 2 – Indicator pair comparison

This method relies on measuring the same cellular response with different indicators. For a single indicator (indicator 1), the relationship between fluorescence and calcium from Equation 1 can be expressed also as:

$$\frac{F_{r(1)}}{F_{0(1)}} = 1 + (R_{f(1)} - 1) \frac{[Ca]_r^{n(1)}}{K_{d(1)} + [Ca]_r^{n(1)}} \quad (\text{Eq. 4})$$

Where F_r is the fluorescence at rest, F_0 is the minimum fluorescence, R_f is the dynamic range of indicator 1, K_d is the affinity constant of the indicator 1, $[Ca]_r$ is the calcium concentration at rest and $n(1)$ is the Hill coefficient of indicator 1.

After stimulation calcium has changed to a new concentration, $[Ca]_s$, which corresponds to a new fluorescence F_s . One can get the ratio of both equations obtaining:

$$\frac{F_{s(1)}}{F_{r(1)}} = \frac{1 + (R_{f(1)} - 1) \frac{[Ca]_s^{n(1)}}{K_{d(1)} + [Ca]_s^{n(1)}}}{1 + (R_{f(1)} - 1) \frac{[Ca]_r^{n(1)}}{K_{d(1)} + [Ca]_r^{n(1)}}} \quad (\text{Eq. 5})$$

A single equation is not sufficient to solve for the values of $[Ca]_r$ and $[Ca]_s$, but the same procedure can be applied to a different indicator (indicator 2)

$$\frac{F_{s(2)}}{F_{r(2)}} = \frac{1 + (R_{f(2)} - 1) \frac{[Ca]_s^{n(2)}}{K_{d(2)} + [Ca]_s^{n(2)}}}{1 + (R_{f(2)} - 1) \frac{[Ca]_r^{n(2)}}{K_{d(2)} + [Ca]_r^{n(2)}}} \quad (\text{Eq. 6})$$

Once fluorescence values at rest ($F_{r(1)}$ and $F_{r(2)}$) and after stimulation ($F_{s(1)}$ and $F_{s(2)}$) are obtained experimentally for the two indicators, the system formed by Equations (5) and (6) contains only two unknowns $[Ca]_r$ and $[Ca]_s$, and values for these can be found numerically with the Newton method. This was done with a custom program written for Mathematica (Wolfram), which can be found at <https://github.com/jaimedejuan/pair-wise-indicator-calcium.git>.

Cytosolic calcium analysis using GCaMP6f or jRCaMP1b

GCaMP6f and jRCaMP1b have nonlinear responses to changes in cytosolic $[Ca^{2+}]$ as previously described in vitro (Chen et al., 2013). To linearize GCaMP6f and jRCaMP1b signals we inverted the Hill equation of fluorescence versus $[Ca^{2+}]$ and used the known in vitro parameters of these indicators to estimate nM changes during activity. Similarly to μM estimates in ER $[Ca^{2+}]$, this conversion relies on the experimental measurement of GCaMP6f and jRCaMP1b fluorescence at saturating $[Ca^{2+}]$, which is obtained by applying Tyrode's solution containing 1 μM ionomycin at pH 6.9 (F_{max}) as previously reported (Hoppa et al., 2012). Baseline cytosolic Ca^{2+} ($[Ca]_{cyto}$) is calculated from F_{max} using the following equation:

$$[Ca]_{cyto} = K_d \left(\frac{F_{cyto}/F_{max} - 1/R_f}{1 - F_{cyto}/F_{max}} \right)^{1/n} \quad (\text{Eq. 7})$$

Where K_d is the affinity constant of the indicator, F_{cyto} is the fluorescence measured at rest, R_f is the dynamic range (F_{sat}/F_{apo}) and n is the Hill coefficient. In general, linearized $[Ca^{2+}]_{cyto}$ (nM) signals are shown in this study as normalized traces to show percentage effects more clearly. In experiments were prolonged stimulation was used, 1 μM ionomycin perfusion was used as a control to ensure that activity-driven responses were not limited by indicator saturation (Figures S4B and S4C).

ER pH measurements

ER pH measurements were made using ER-targeted pHluorin (pKa 7.1) expressed in neurons and imaged at neuronal somas or pre-synaptic varicosities identified by VAMP-mCherry expression. Neurons were briefly perfused with a Tyrode's solution containing 100mM NH₄Cl buffered at pH 7.4 and 7.8 using 25mM HEPES, which equilibrated ER pH to 7.4 or 7.8 after a transient overshoot

of fluorescence (Figure S2C) as previously described (Kim et al., 1998). The fluorescence value when pH stabilizes at 7.4 or 7.8 allows estimating resting ER pH (Figure S2D) value using the modified Henderson-Hasselbalch equation:

$$pH = pK_a - \log \left[\left(\frac{1 + 10^{pK_a - pH(NH_4Cl)}}{\frac{F_0}{F_{NH_4Cl}}} \right) - 1 \right] \quad (\text{Eq. 8})$$

pK_a is the pK_a of pHluorin, 7.1, $pH(NH_4Cl)$ is the pH of 100mM NH₄Cl buffer used, F_0 is the fluorescence of ER pHluorin measured before NH₄Cl perfusion, F_{NH_4Cl} is the fluorescence of ER pHluorin measured upon NH₄Cl perfusion when signal is stable. Final pH value obtained per cell is the average of 7.4- and 7.8-based estimates.

Analysis of correlation between $[Ca^{2+}]_{ER}$ and single AP Ca^{2+} entry

To examine the putative correlation between $[Ca^{2+}]_{ER}$ and single AP Ca^{2+} entry we assumed a monotonic relationship between the two variables and calculated the Spearman's correlation coefficient (ρ) of our raw datasets (presented in Figures S6A and S6B) using R (R Development Core Team). To reduce observational noise, we binned our raw data using a bin size of $[Ca^{2+}]_{ER} = 25 \mu M$ starting from $75 \mu M$. Errors of binned data points for $[Ca^{2+}]_{ER}$ and 1AP jRCaMP1b responses were calculated by summing in quadrature the experimental estimates of the error for each individual data point. We used the binned dataset (presented in Figure 6) to fit our data with better accuracy. A Hill equation fit was selected because 1) reported less error in the determination of the equation parameters as well as a better adjusted R-square value (Adj R-sq = 0.87) and 2) is in agreement with previously published studies showing that STIM1 activation presents high cooperativity well described by a Hill equation (Luik et al., 2008; Stathopoulos et al., 2008; Zheng et al., 2011). The Hill model was fitted with statistical weights using Origin 8.0 (LabCorp).

Estimates of contributions of ER efflux to resting cytosolic Ca^{2+}

Although signals in axons are small the reported affinity of GCaMP6f ($K_d = 375 nM$) should be in the correct range to assess changes in resting calcium. Our procedures used to linearize the GCaMP6f response also allow us to estimate the resting Ca^{2+} since we know the in-vitro properties of the indicator. These calculations predict that the resting Ca^{2+} concentration in axons is $\sim 120 nM$ (in both axons and dendrites). One can then ask how large the fluctuations are in the baseline to get a sense of how much the signal would have to change in order to see something meaningful. The standard deviation of the baseline (Figure S1D) represents a $\Delta F/F \sim 0.01$ and corresponds to a fluctuation of resting Ca of $\sim 1.1 nM$. By comparison a single AP transiently elevates the average bouton Ca^{2+} to $9.6 nM$ ($\Delta F/F$ signal ~ 0.07), and the CPA induced changes in the dendrite correspond to an elevation of $11.8 nM$ ($\Delta F/F = 0.08$). This demonstrates that GCaMP6f is easily capable of detecting similar changes in axons and, therefore, we feel it is justified to conclude that SERCA block does not result in increased baseline cytosolic calcium in the axon. We suspect that the difference observed is a consequence of a different ratio between ER volume and cytoplasmic volume - whereas dendrites likely have elaborated ER networks, axonal ER appears to be much simpler and might occupy less % of the total cytoplasmic volume.

Statistics

Error bars indicate mean \pm SEM unless otherwise noticed. Box whisker plots represent median (line), mean (point), 25 - 75 percentile (box), 10 - 90 percentile (whisker), 1 - 99 percentile (X) and min - max (—) ranges. Statistical analyses were performed by one-way ANOVA followed by Tukey's multiple comparisons test except for paired data (e.g., before and after CPA) where paired t test was used to compare. When analyzing correlation, the Spearman's correlation coefficient (ρ) was considered significant if $p < 0.05$. For other analyses $p < 0.05$ was considered significant and denoted with a single asterisk, whereas $p < 0.01$, $p < 0.001$ and $p < 0.0001$ are denoted with two, three, and four asterisks, respectively. The sample replicate number (n) referred to in all figures represents individual cells of a given treatment condition.

Analysis of the samples was not blinded to genotype. Strategies for randomization, replication and sample-side estimation are not applicable to the study.

DATA AND SOFTWARE AVAILABILITY

A custom program written for Mathematica (Wolfram) to easily propagate errors on ionomycin-based ER calcium estimates can be found at <https://github.com/jaimedejuan/Error-propagation-ER-Ca>.

A custom program written for Mathematica (Wolfram) to estimate baseline ER calcium by comparing responses from 2 different indicators can be found at <https://github.com/jaimedejuan/pair-wise-indicator-calcium.git>.

The ImageJ plugin Time Series Analyzer V3 is available at <https://imagej.nih.gov/ij/plugins/time-series.html>.